3D instantaneous dynamics modelling of the surface motion associated with East European subduction zones

MSc Thesis Research
A.J. (Bert) van Amerongen
5723272
7 July 2023

Supervisors
Prof. Dr. Wim Spakman
Prof. Dr. Cedric Thieulot

In collaboration with
Lex Verbrugh MSc
Erik van der Wiel MSc

Abstract

Forecasting earthquakes is a prime future target of Solid Earth research to which geodynamics research can contribute by providing a deep understanding of the physical drivers generating the lithosphere stress driving earthquakes. Processes confined to the lithosphere are known to cause stress build-up. However, the contribution of the Earth's mantle is less substantiated. Assessing the contribution of deep dynamic drivers to lithosphere deformation can be done by numerical modelling by creating predictions of deformation that are then tested against observations, e.g., the GNSS surface motion field.

Here we present the findings of 3D geodynamic modelling of the Vrancea (east Carpathians) and Aegean subduction zones in south-eastern Europe. Two differing tectonic settings - in Vrancea seismically active continent-continent collision and in the Aegean roll-back subduction- of differing scale are present, providing a suitable case to test interplay of mantle drivers and their effect on surface/crustal flow. To this end a 3D initial temperature-density model is designed from published lithospheric thickness and tomography models down to a depth of 800 km. We solve the equations describing the conservation of mass and momentum pertinent to a viscoplastic continuum, using the finite-element code ASPECT (Kronbichler, Heister and Bangerth 2012). Surface motion predictions from these models are then validated against the observed GNSS field (Global Navigation Satellite System, such as the Global Positioning System (GPS)). First a reference model is constructed that shows a good first-order fit of the crustal flow field, namely the characteristic westward movement of Anatolia and a rotation to the SW of the Aegean region towards the Hellenic trench. Predictions of the flow in the upper mantle show that the surface flow is correlated to the predicted mantle flow pattern and models without the Aegean slab fail to explain the rotation of the Aegean region. Experiments on the seismically active Vrancea slab cannot show differences in predicted surface observables between a slab that is continuous or a detached slab, but the models predict that a continuous slab experiences more resistance from the mantle against slab dragging by the Eurasian plate which could increase seismic activity. Second, experiments are performed to determine the sensitivity of the surface flow field for the make-up and rheology of the lithosphere and slabs. Potential model improvements such as STEP faults and a rheologically heterogeneous Eurasian plate are explored. Furthermore, the 3D models provide novel insight into the correlation between mantle flow and the pattern of seismic mantle anisotropy in subduction zones, as well as the 3D interaction between mantle flow, basal tractions on the lithosphere and tectonic plate motions. This research provides a steppingstone to more detailed studies of subduction plate boundary regions, which may lead to a better understanding of the physical drivers of crustal deformation and flow and may provide constraints for future seismic-hazard modelling.

Introduction

Mechanical stress within the Earth's lithosphere causes earthquakes. The amplitude of stress is not directly measurable, but it can be predicted from a 3D geodynamical model of (a part of) the Earth. A model useful for stress field analysis would correctly predict various observations of crustal deformation, particularly the observed variable motion of Earth's surface. The buildup of lithosphere stress in plate tectonic settings is ultimately a combination of lithosphere and mantle drivers. The geodynamic drivers confined to the lithosphere have been thoroughly investigated using models that are confined to the lithosphere domain, for instance for the complex tectonic setting of the eastern Mediterranean region (e.g. Carafa et al., 2015; England et al., 2016; Göğüş et al., 2016; Özbakir et al., 2017; Warners-Ruckstuhl et al., 2012). In such modelling, the specific contribution of mantle processes, i.e., mantle flow and lithosphere subduction and its interaction with the ambient mantle, to lithosphere stress buildup is absent or underrepresented and warrants closer investigation.

In this MSc thesis, Eastern Europe, encompassing the Pannonian-Carpathian region and the Aegean-West-Anatolia region, is chosen as the natural laboratory to investigate the effect of mantle drivers to surface deformation by 3D geodynamic crust-mantle modelling (Figure 1.1, 1.2). The Carpathian mountain belt and Hellenic arc are the surface signatures of two important plate tectonic settings. The Carpathians are an orogen resulting from a slow continent-continent convergence (e.g. Cloetingh et al., 2004; Faccenna et al., 2014; Schmid et al., 2020; van Hinsbergen et al., 2020) and the Hellenic arc is a slow-convergence subduction system experiencing roll-back (e.g. Wortel and Spakman 2000; Jolivet et al., 2013; Schmid et al. 2020).

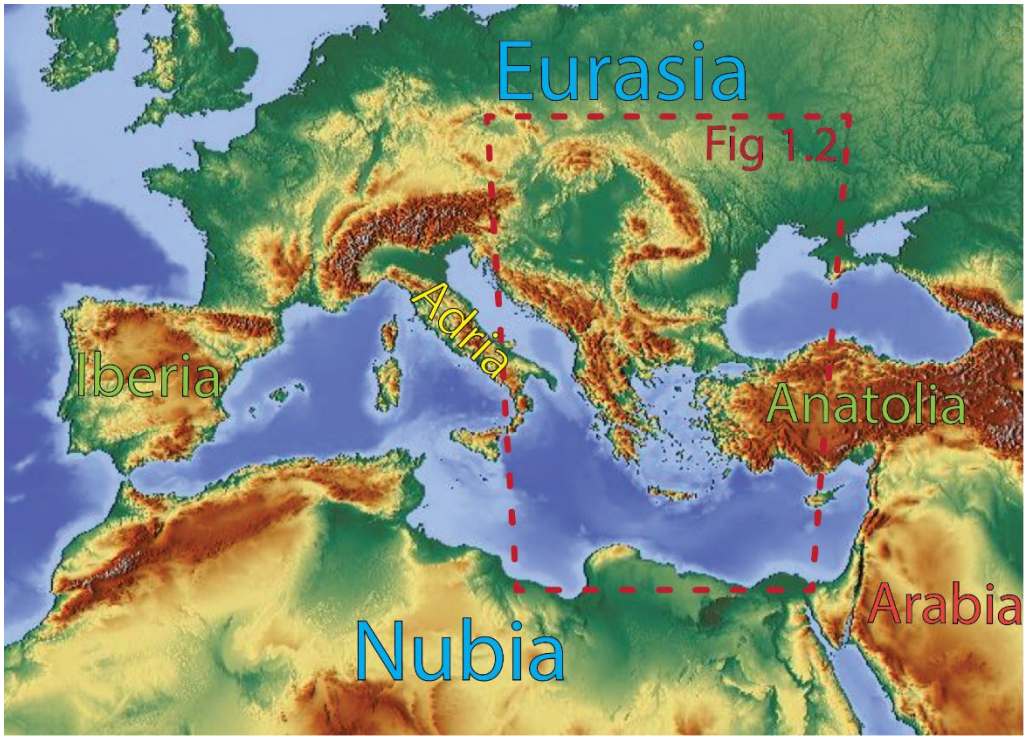

Figure 1.1 Topographical map of the Mediterranean Sea. Source: maps-for-free

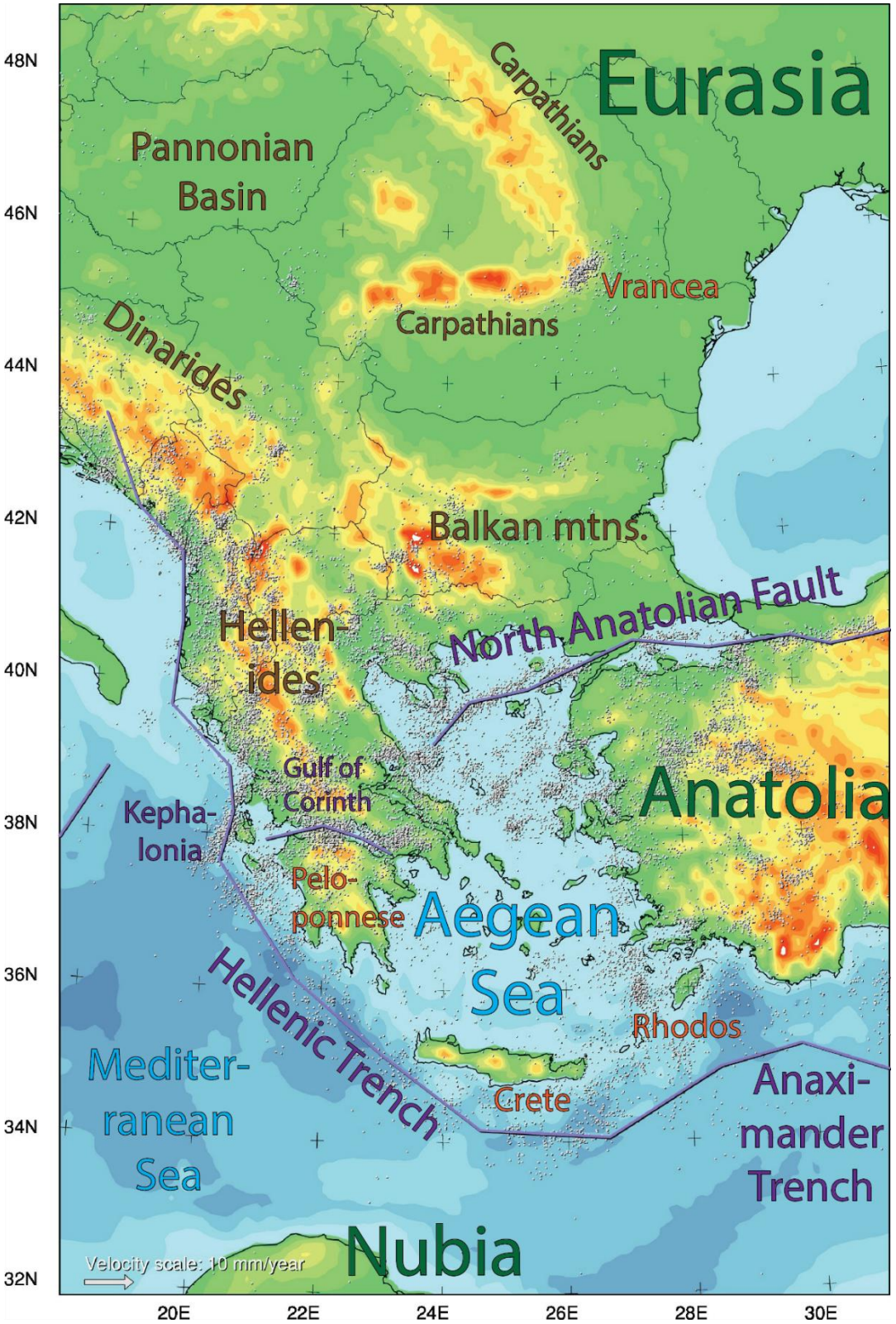

Figure 1.2 Map of the model domain with dots exemplifying the earthquake occurrence (source: International Seismological Centre).

The Vrancea slab at the SE corner of the Carpathians is a location of significant intracontinental earthquakes, yet the type of tectonic setting producing these earthquakes remains elusive (Fuchs et al., 1979)(Figure 1.2). Many arguments for crustal delamination (Gîrbacea and Frisch, 1998; Knapp et al., 2005), a subducting slab (e.g. Bokelmann and Rodler, 2014; Sperner et al., 2001), and whether the slab is continuous or detached have been provided (Koulakov et al., 2010; Petrescu et al., 2021) but are not yet in agreement. Recent research alludes that added compression from ambient mantle flow could cause this anomalous seismicity (Petrescu et al. 2021), a hypothesis that can be examined by 3D geodynamical modelling that includes slab-mantle interaction.

The Hellenic arc has been widely investigated by geological, geodynamical, and seismological research (summarized by Faccenna et al. 2014). Outstanding questions comprise the morphology and composition of the Aegean slab. This feature extends into the lower mantle (Bijwaard et al., 1998; Spakman et al., 1993) and laterally extends from the NW-Greece to its eastern slab edge under western Anatolia (De Boorder et al. 1998). Details of Aegean slab age, composition, and rheology are ill-constrained. The slab's tomographic image below the Hellenides between 200-400 km depth offers multiple interpretations, creating a dichotomy between a horizontal tear (Wortel and Spakman, 2000) or an slab segment of a different (i.e. continental) type (van Hinsbergen et al. 2005). Additionally, possible lateral transitions in slab morphology exist, e.g., reflected by the Kephalonia fault and a slab edge under Rhodos (Govers and Wortel, 2005; Özbakır et al., 2020), of which the impact on the regional surface and mantle flow field are still largely unclear.

Studies up to now were mostly conducted with 2D elastic/viscous sheet modelling (e.g. Bird, 1998) The method is computationally efficient compared to 3D crust-mantle modelling and its merits are summarized in Carafa et al. (2015). 3D modelling has more unconstrained natural properties, the vertical composition and rheological makeup of the lithosphere is more important in a full 3D description but may not provide much additional information when compared to the results of 2D modelling (Bendick and Flesch, 2013) and for large-scale deformation the 2D thin sheet approximation is considered appropriate (Lechmann et al., 2011). However, these models require boundary tractions usually imposed on plate boundaries including subduction trenches which is presumably complex due to the impact of the slab's sinking effect, the coupling between overriding and subducting plate, and the tractions of the mantle acting at depth on the slab. Additionally, boundary tractions along the other edges have to be either assumed or become tunable parameters (e.g. Carafa et al. 2015, England et al. 2016). Finally, this type of model cannot discriminate between active (convective) and passive (plate motion friction) basal shear tractions. A hybrid approach is to compute mantle tractions acting on the base of thin-sheet models from a separate mantle convection simulation but this involves an approximate approach to match the pressure between lithosphere model and mantle model (Warners-Ruckstuhl et al. 2012). These approximations and problems can all be avoided when using a full 3D crust-mantle modelling approach (e.g., Glerum et al. 2019).

From these various model designs several conflicting conclusions have developed regarding key drivers which are difficult to reconcile. 2D thin sheet models were able to explain the Aegean-Anatolia crustal flow field based solely on GPE-gradients and model boundary tractions (England et al. 2016), in which differences in lithostatic pressure, with its minimum on the African plate in the Mediterranean Sea (GPE sink) and the maximum in central Anatolia (GPE source) lead to the characteristic SW-ward flow of the crustal flow field, disregarding the observed collisional effect of Africa deflecting the Aegean and Eurasia NE-ward (Warners-Ruckstuhl et al. 2012). Carafa et al. (2015) explain the motion of the Aegean-Anatolia microplate by the interplay of inter-plate and basal tractions. The retreat of the slab results in a return flow, inducing trench oriented basal shear and a gradient in the lithosphere thickness. This basal traction and pressure gradient together balance the compression by the collision of Africa in this model.

The merit of 3D geodynamic modelling in a mantle reference frame is that it can incorporate all physical processes of the lithosphere and mantle and explicitly discriminates between active (convectional) and passive (resistance to plate motion) shear tractions at the base of the lithosphere. Additionally, it will create a steppingstone for future 3D models towards more realistic numerical models.

Here, we build on developments of instantaneous 3D geodynamic crust-mantle modelling initiated by Glerum et al. (2019). We use the novel Geodynamic World Builder (Fraters et al., 2019) to construct the complex 3D temperature and density structure appropriate for the unique tectonic setting that will be input of the geodynamic modelling. This tool allows for rapid design of tectonic plates, weak zones mimicking plate boundaries, and 3D slab geometry. The tool is integrated in the open source numerical finite element code ASPECT (Kronbichler et al., 2012).

This research 1) aims to create a new 3D temperature-density model of Eastern Europe and the Aegean region for geodynamic modelling. 2) By experimenting with model rheology, this model is then refined to a reference model that provides a reasonable fit to the GNSS observed surface flow field. The dynamic coupling between the mantle and surface deformation will be evaluated from 3) a sensitivity analysis of the model to find the mantle dynamic drivers for the first-order characteristics of the surface flow field of Eastern Europe & the Aegean-West-Anatolian regions. Lastly, 4) it aims to address regional geodynamic questions on how far north the dynamic effect of the Aegean slab roll-back reaches, and what the impact of the Vrancea slab is on the local flow field.

We start by describing the region's lithosphere-mantle structure and the surface kinematics. Next, we present the governing geodynamic equations, the numerical solver ASPECT and the construction of the complex initial conditions using the Geodynamic World Builder & the tomographic model UU-P07 (Amaru, 2007), and the model boundary conditions. An initial batch of experiment leads to a reference model which is next used for sensitivity tests by varying model properties to illustrate the response of the predicted surface flow field and to search for model improvements.

Geodynamic setting

General geography

The present plate-tectonic configuration of Mediterranean & Eastern European regions (Figure 1.1, 1.2) are ultimately a result of the closure of the Tethys ocean since Mesozoic time (Handy et al., 2010; van Hinsbergen et al. 2020). The closure of the ocean is in its final stages and convergence has slowed to a pace where roll-back and back-arc basin development is dominant (Wortel and Spakman 2000, Jolivet et al., 2013). This study focuses on two active geodynamic systems: the Vrancea subduction at the SE of the Carpathian mountain range and the Hellenic subduction below the Aegean region. The northern end of the arcuate Carpathian mountain range starts in Slovakia, curves southeastward into Romania where it strongly bends southwestward into Serbia and connects in the south with the Balkans, Hellenides and Dinarides. The Vrancea subduction system in the SE is the only presently active part of the Carpathian arc. The Hellenic trench is the site where the African plate subducts below Eurasia. It traces from the Cyprus and Antalya subduction zones in the east westward along the south of the accreted wedge islands Rhodos and Crete, northwestward along Peloponnese, the Hellenides mountain range and further along the east coast of the Adriatic sea at the base of the Dinaride mountain range.

Plate convergence and crustal motions

The region is characterized by three domains: the Eurasian plate, the African (Nubian) plate and the Aegean-Anatolia microplate. The convergence between the large continents Eurasia and Africa is oriented about NW-SE with a magnitude of ~5.5 ±0.5 mm yr^{-1} at the latitude of Cyprus, decreasing to ~4.4 ±0.3 mm yr^{-1} at the latitude of Algiers (Nocquet, 2012). Within the Eurasian plate southward motion is observed in the Balkan mountain range and mainland Greece relative to a fixed Eurasia (Figure 2.1). The sparse dataset north at the Carpathians and the Pannonian basin shows a coherent movement with the rest of Eurasia.

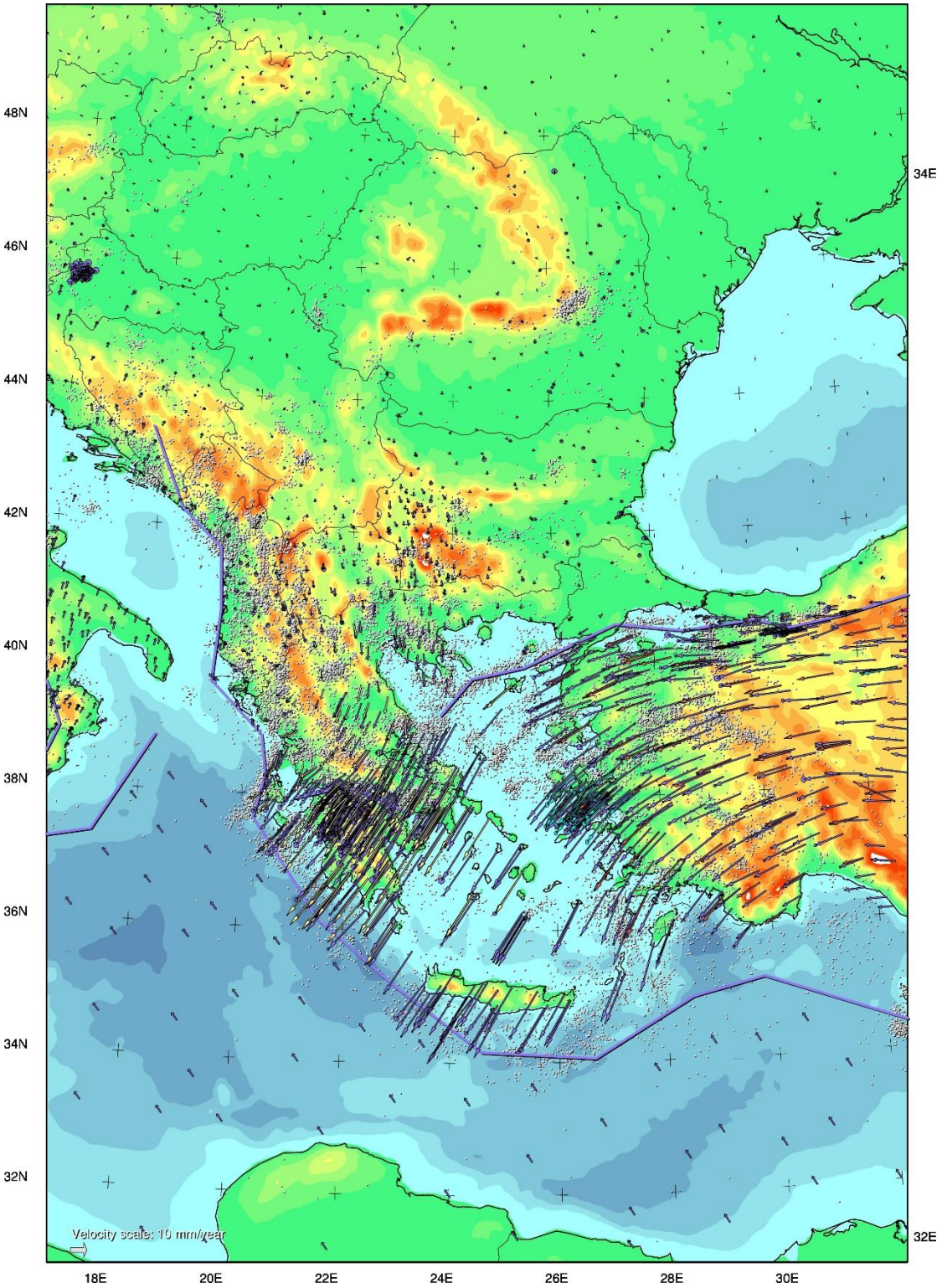

Figure 2.1 GNSS field of the Carpathians-Aegean region (Kreemer et al., 2014; Métois et al., 2015; Piña-Valdés et al., 2022; Serpelloni et al., 2022). Synthetic motion vectors in the Eastern Mediterranean Sea show the motion of Africa relative to Eurasia.

The movement of the Aegean-Anatolia microplate is more complex. GNSS stations across the area display a dominant westward movement of the microplate Anatolia, rotating to a south-west, trench-perpendicular motion within the Aegean Sea in a Eurasia-fixed

reference frame (Figure 2.1). The boundary between the Aegean-Anatolia microplate and Eurasian continent is the North Anatolian Fault (Figure 1.2). This prominent strike-slip fault traces from the north of the Anatolian microplate westward, passing just south of Istanbul and terminating in the north Aegean Sea. This fault accommodates all of the relative Eurasia-Anatolia movement (McClusky et al., 2000; Nocquet, 2012). Further tectonic weak zones can be traced along the Gulf of Corinth.

Hellenic subduction system

The African plate subducts below the Aegean-Anatolia microplate and Eurasian plate along the Hellenic trench. The subducting slab has been well imaged (Piromallo and Morelli, 2003; Spakman et al., 1993, 1988; van der Meer et al., 2018; Wortel and Spakman, 2000)(Figure 2.2). In the east Mediterranean, the slab is segmented into the Cyprus slab in the east, the Antalya slab in the center and the larger Aegean slab further to the west (Berk Biryol et al., 2011; De Boorder et al., 1998)(Figure 2.3). The slab curves in an amphitheater style around the Aegean to a maximum depth of 1500 km (Bijwaard et al. 1998; van der Meer et al. 2018) consisting of intermittently oceanic and continental lithosphere (van Hinsbergen et al., 2005). Beneath Albania, the maximum depth of the slab decreases to ~150-180 km (Handy et al., 2019). This relatively short slab persists below and along the east Adriatic coast, following the Dinarides to the NW, at a maximum depth of 150-200 km (El-Sharkawy et al., 2020).

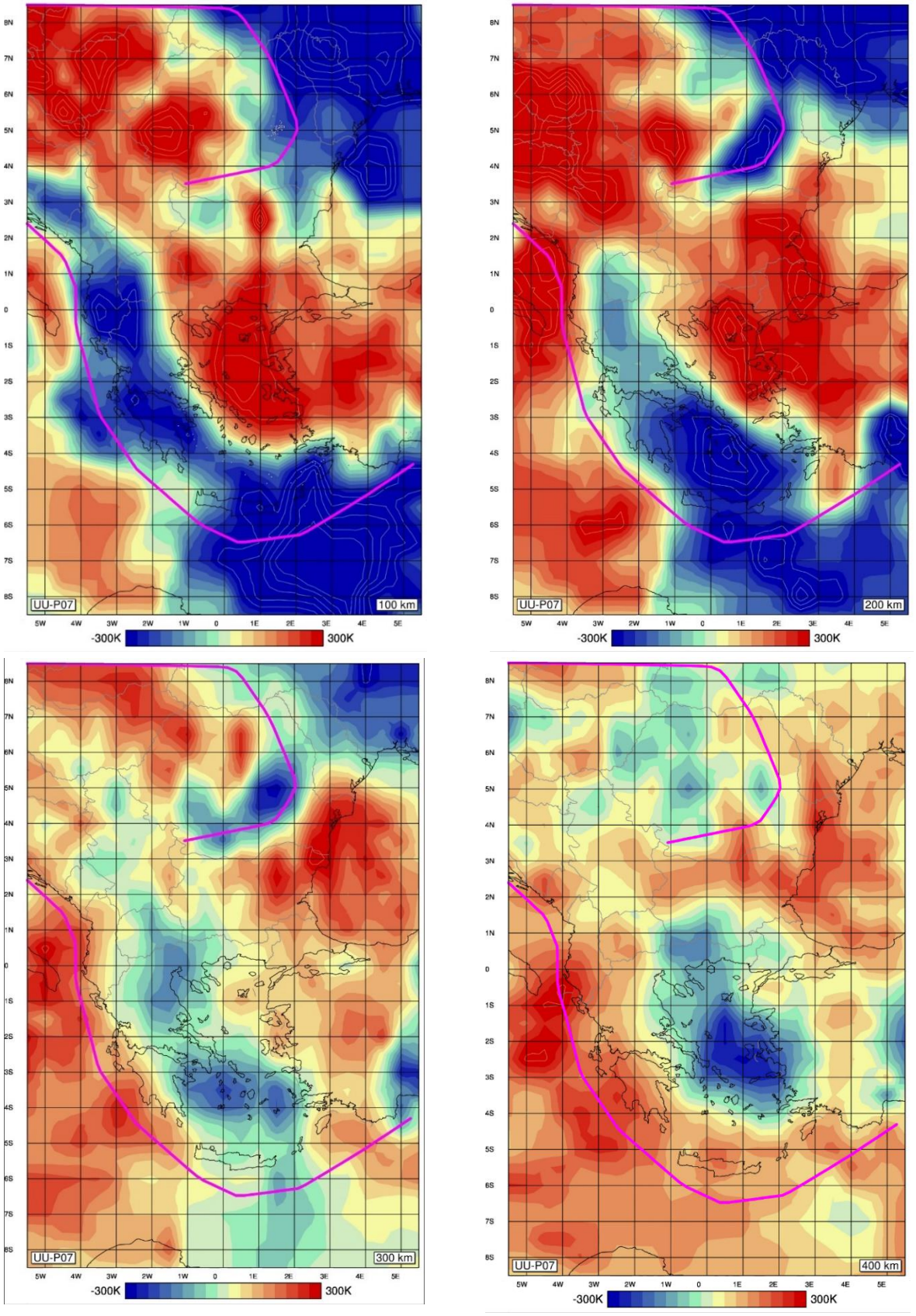

Figure 2.2 Tomographic slices of model UU-P07 (Amaru 2007) for various depths, converted to temperature anomalies. The subduction interfaces are highlighted in purple. The longitude-latitude grid belongs to the rotated spherical frame with the origin in 40.5N 24.5E.

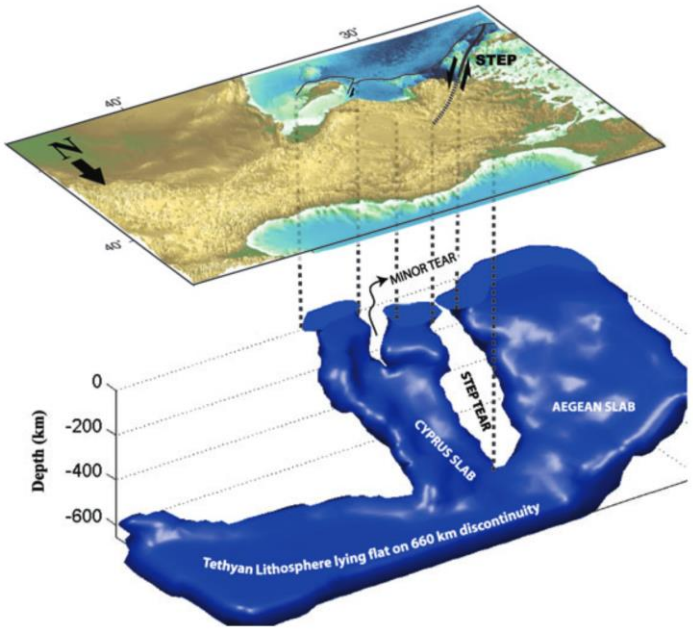

Figure 2.3 Synthesis of the morphology of the Aegean (right), Antalya (center) and Cyprus (left) slabs (Berk Biryol et al. 2011)

The overriding plate in this subduction system is the Eurasian plate, particularly the Aegean-Anatolia platelet. Anatolia consists of four domains: the contractional East Anatolian, the North Anatolian, the Central Anatolian and the extensional West Anatolian province (Berk Biryol et al. 2011, and references therein). Crustal thicknesses are ~ 30 km for the west domain and ~ 35 km for the north and central domain (Karabulut et al., 2019), and the lithosphere is generally thinned. The Aegean sea lies in a back-arc basin that has been extended by southward roll-back of the Aegean slab since Eocene times (e.g. Brun et al., 2016; van Hinsbergen and Schmid, 2012), with a total of 400 km trench-perpendicular extension and 650 km trench-parallel extension, and is highly heterogeneous in crustal strength (Jolivet et al. 2013). This resulted in a thinned Aegean lithosphere of ~40-60 km based on surface wave dispersion (Endrun et al., 2011). The Africa-Eurasia contact is traced by the Hellenide and Dinaride mountain ranges. Below the Dinarides, the crustal thickness is 40 km and decreasing to 30 km below the Moesian platform (Marović et al., 2002).

Vrancea slab

The Carpathians are the intracontinental mountain belt in Romania that connects the Ticia-Dacia microplate (Gîrbacea and Frisch, 1998) and the East Europe craton. It formed during continental collision in middle Miocene times and its collision peaked at 8-9 Ma (Matenco and Radivojević, 2012). The south-east corner of the Carpathians is our area of interest, as a high-velocity seismic anomaly with high seismicity was discovered. This region close to the Romanian capital Bucharest produces intense earthquakes (Oncescu and Bonjer, 1997) despite its large distance from present day plate boundaries.

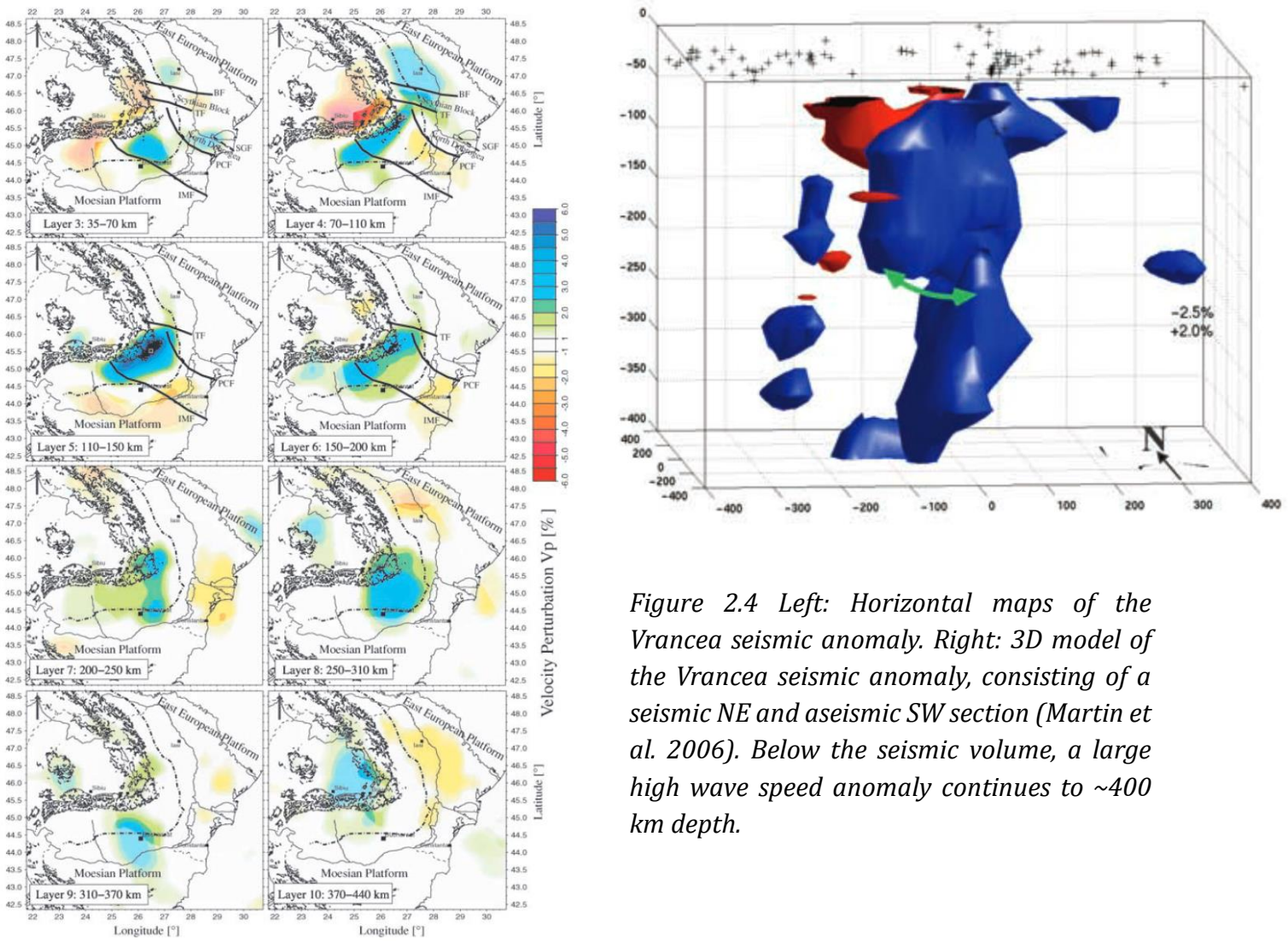

Figure 2.4 Left: Horizontal maps of the Vrancea seismic anomaly. Right: 3D model of the Vrancea seismic anomaly, consisting of a seismic NE and aseismic SW section (Martin et al. 2006). Below the seismic volume, a large high wave speed anomaly continues to ~400 km depth.

The high-velocity anomaly has progressively been imaged in higher resolution (Figure 2.2, 2.4) (Baron and Morelli, 2017; Bokelmann and Rodler, 2014; Koulakov et al., 2010; Martin et al., 2006; Weidle et al., 2005; Wortel and Spakman, 2000). First imaged by Wortel & Spakman (2000), they infer a subducted slab that is in a state of detachment. The anomaly consists of a seismic NE section and an aseismic SW section (Martin et al.

2006). The seismic section is limited to a small volume at intermediate depth recognized as an ‘earthquake nest’, a feature usually found in continental collision settings with previous oceanic subduction but presently removed from active convergent margins (Fuchs et al. 1979, Oncescu et al. 1997). Above the anomaly exists a vertical gap in seismicity at 40 – 70 km depth, which has been attributed to a detached oceanic slab (Fuchs et al. 1979).

The nature of the high-velocity anomaly in the Vrancea zone is under debate. As noted by Bokelmann & Rodler (2014), seismic tomography cannot distinguish between the two leading options: subducted lithosphere (oceanic or continental) or delaminated lithosphere. Arguments for delaminated continental lithosphere are borehole logs showing continental crust in locations incompatible with oceanic subduction (Knapp et al. 2005) and (Gîrbacea and Frisch, 1998) recognize the match between a 130 km horizontal gap in the lower crust (between epicentral of the earthquake nest and the Miocene suture zone) with the 70-200 km deep earthquake nest volume. The case for subducted oceanic lithosphere is argued in (Sperner et al., 2001) and Bokelmann & Rodler (2014). There are also arguments for a hybrid where continental delamination occurred after subduction, leading to a steep slab and an upwelling of the asthenosphere NW of the subduction zone (Girbacea & Frisch 1998). Additionally, there is discussion whether the anomaly is continous or detached from the overlying lithosphere. P- and S-wave tomography shows that the earthquake nest starts at a depth of~ 60 km in a low velocity zone, 30 km above the fast anomaly (Koulakov et al. 2010) implying a possible detachment between the anomaly and overlying lithosphere.

Methods

Overview & aim

We design a 3D instantaneous dynamics model excited by thermal density perturbations. Firstly we describe the numerical formulation and used numerical solver. Secondly, the domain and its imposed boundary conditions are expanded upon. Thirdly, we elaborate on the design and implementation of our custom complex initial temperature-density conditions. Finally, we provide a description of the material parameters and deformation mechanisms.

Numerical formulation

The instantaneous flow problem posed in this thesis are solved by the Finite Element Model ASPECT, the Advanced Solver for Problems in Earth's ConvecTion (Kronbichler, Heister and Bangerth 2012). The physical flow laws that are solved are (1) the momentum conservation equation, (2) the continuity of mass equation for compressible flow and (3) conservation of energy. (4) describes how the compositional fields are advected.

$$-\nabla \cdot \left[2\eta\left(\dot{\varepsilon}(\boldsymbol{u}) - \frac{1}{3}(\nabla \cdot \boldsymbol{u})\boldsymbol{I}\right] + \nabla p = \rho \mathbf{g} \tag{1}$$

$$\nabla \cdot (\rho \boldsymbol{u}) = 0 \tag{2}$$

$$\begin{aligned} \rho C_p \left(\frac{\partial T}{\partial t} + \boldsymbol{u} \cdot \nabla T\right) - \nabla \cdot k \nabla T &= \rho H \\ &+ 2\eta\left(\dot{\varepsilon}(\boldsymbol{u}) - \frac{1}{3}(\nabla \cdot \boldsymbol{u})\boldsymbol{I}\right) : \left(\dot{\varepsilon}(\boldsymbol{u}) - \frac{1}{3}(\nabla \cdot \boldsymbol{u})\boldsymbol{I}\right) \\ &+ \alpha T(\boldsymbol{u} \cdot \nabla p) \\ &+ \rho T \Delta S \left(\frac{\partial X}{\partial t} + \boldsymbol{u} \cdot \nabla X\right) \end{aligned} \tag{3}$$

$$\frac{\partial c_i}{\partial t} + \boldsymbol{u} \cdot \nabla c_i = q_i \tag{4}$$

Here η is viscosity (Pa s), $\dot{\varepsilon}$ is the strain rate tensor (s^{-1}), $\boldsymbol{u}$ is the velocity vector (m s^{-1}), p is the pressure (Pa), ρ is the mass density (kg m^{-3}), $\mathbf{g}$ is the gravity vector (m s^{-2}), C_p is the heat capacity (J K^{-1}), T is temperature (K), t is time (s), k is the thermal conductivity (W $m^{-1}K^{-1}$), H is the radiogenic heat production, α is the thermal expansion coefficient (K^{-1}), ΔS is the entropy change, X is the material fraction related to phase change, c_i describes the compositional fields used and q_i is the allowed reaction rate between materials. Equations (3) and (4) are added for completeness but does not bear further consideration in this instantaneous model.

Domain

The Aegean and Vrancea region are captured in a spherical chunk (Figure 3.1) The curved rectangular surface has its origin in 40.5N 24.5E. The domain spans from -5.5 to +5.5 local longitude and -8.5 to +8.5 local latitude. The model is 800 km deep and is subdivided in an outer and inner chunk at 120 km depth (elaborated upon in the section on boundary conditions). This domain is discretized by an adaptive mesh (Figure 3.2). The base

resolution is a near-cubic chunk with sides of ~30 km. Two additional levels of refinement are imposed on the slab, lithosphere and plate boundary faults. This increases their resolution to near-cubic chunks with sides of ~7 km.

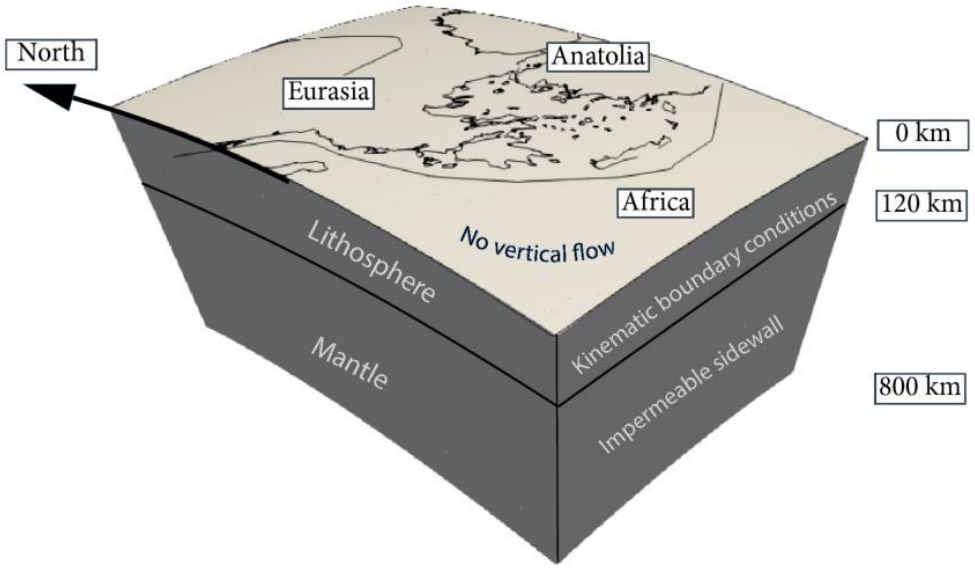

Figure 3.1 Model domain.

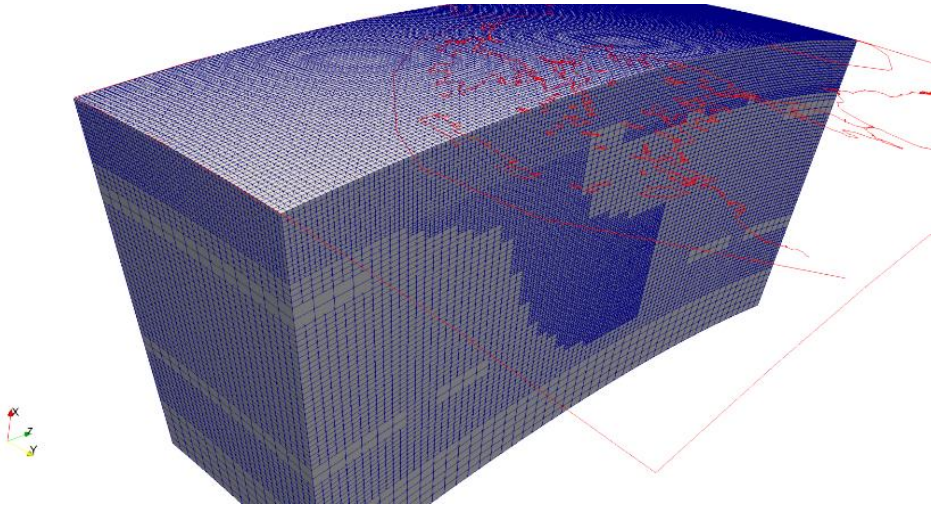

Figure 3.2 Adaptive mesh for a representative cross section of the model (N-S through Crete).

Boundary conditions

The boundary conditions of the model are summarized in Figure 3.1. The surface of the model allows perpendicular flow but no vertical movement. This choice was made to restrict the complexities introduced when allowing for topography and topography changes.

The sidewalls of the inner chunk are also impermeable, which is an unrealistic constraint for subduction zone evolution (Chertova et al., 2012) but poses a stable and predictable condition for our instantaneous model.

The boundary conditions on the outer chunk are kinematic. The African plate motion is adopted from the Global Mantle Hotspot Reference Frame (GMHRF) (Doubrovine et al., 2012) averaged over the past 10 Myr which is defined by the Euler pole (lon, lat, deg/My) = (-33.28, 36.66, 0.1608). The motion of Eurasia is determined by adding the relative Eurasia-Africa Euler pole in ITRF2014 (Altamimi et al. 2017) to the African GMHRF pole leading to (-38.02, 55.27, 0.1232). The GMHRF pole of Anatolia is (27.94, 34.13, 1.196) and is obtained from the relative Euler pole of Central Anatolia relative to Africa, which is obtained from an analysis of the central Anatolian GNSS field (Spakman, personal communications) and is next added to the absolute motion of Africa.

The Eurasia plate motion boundary conditions are imposed from the Dinarides in the west, along the north boundary to the NAF in the east. Here, the Anatolia boundary conditions are imposed between the NAF and the Antalya trench. The Africa boundary conditions are imposed at the Antalya trench, along the south edge to the Dinarides in the west. The boundary conditions are imposed and linearly scaled down between 0 and 120 km depth using the ratio (6371-depth)/6371. To maintain mass preservation under the prescribed convergence within the model domain, a net outflow is imposed on the bottom of the model that compensates the total inflow in the outer chunk.

Complex initial temperature-density conditions

We use the Geodynamic World Builder (Fraters et al. 2019) to design the complex initial conditions of our physical problem (Figure 3.3). The model space consists of two layered compositional fields (the upper and lower mantle) and three laterally varying compositional fields (the lithosphere, weak zones and the subducting slabs, Figure 3.4). The upper mantle resides between the Lithosphere Asthenosphere Boundary (LAB, varying in depth) to 660 km depth. The lower mantle resides between 660 km depth and 800 km depth.

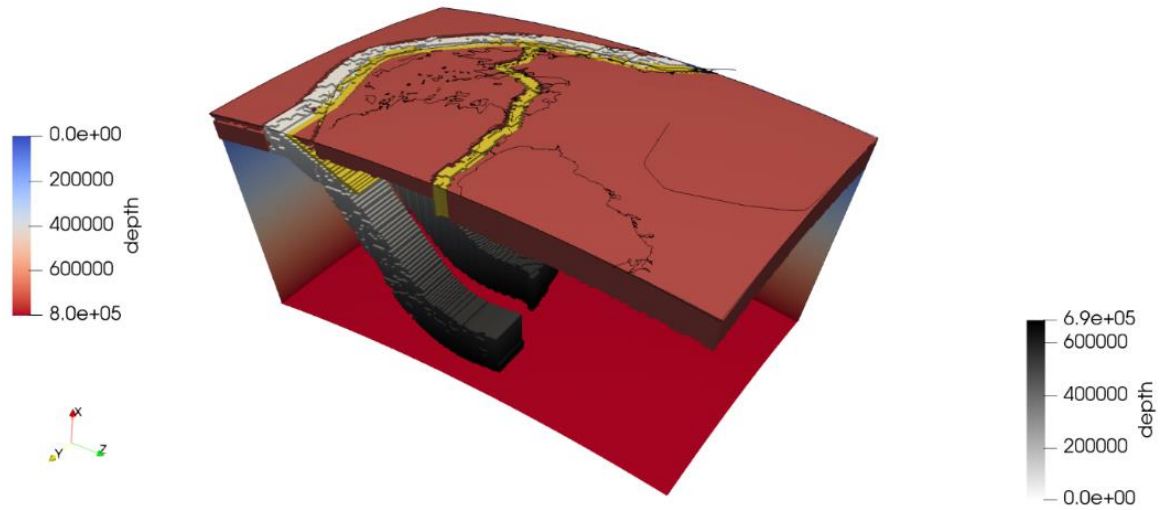

Figure 3.3 Model domain with the three laterally varying layers shown (see Figure 3.4). Red: lithosphere, Yellow: weak zones, White-black: slab. Sidewalls and model floor are shown in blue-red (depth).

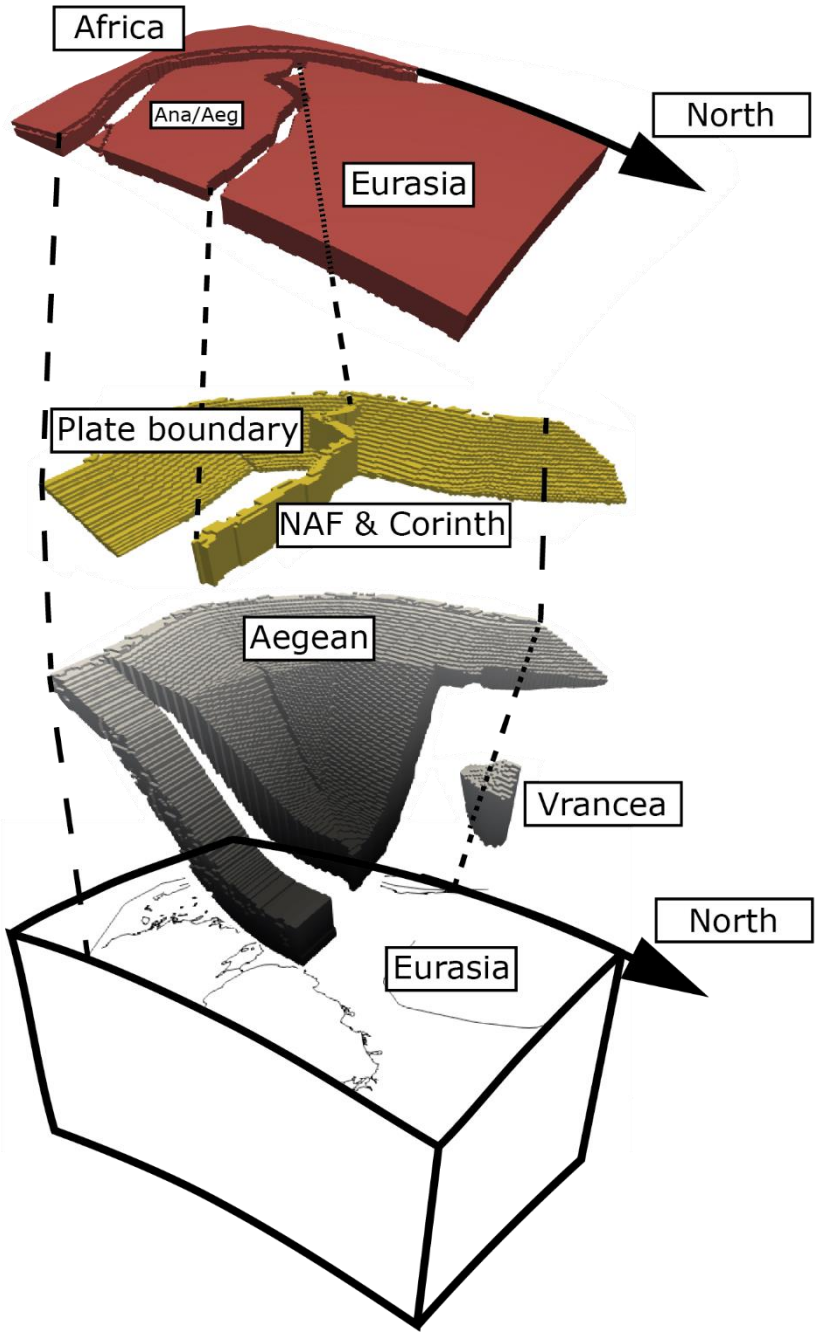

Figure 3.4 Detailed expansion of the three laterally varying compositional fields.

The lithosphere is subdivided into the Eurasian, the Aegean-Anatolia and African plates (Figure 3.4) with a maximum depth of 120 km, 60 km and 100 km, respectively. Its composition is homogeneous (described in this chapter's final section). Two weak zones separate these lithosphere domains. The plate boundary fault along the Hellenic trench is represented as a 30 km thick weak zone, following the geometry of the trench and reaching a maximum depth of 120 km following the varying dip of the slab. The North Anatolian Fault is represented by a 50 km wide vertical weak zone also reaching a

maximum depth of 120 km. This weak zone continues SW and connects via the Gulf of Corinth to the plate boundary weak zone.

Slab morphology

Figure 3.5 shows the morphology of the Dinarides-Aegean-Antalya slab (Aegean slab for short), and the Vrancea slab. Its design is informed by the tomographic model UU-P07 (Amaru, 2007; Hall and Spakman, 2015) and earthquake hypocenters. The choice was made to use UU-P07 for its high resolution and distinct transitions for features ~100-200 km thick. This choice was made after also consulting other (P- and S-wave) models using SubMachine (http://www.earth.ox.ac.uk/~smachine/cgi/index.php). Slab temperatures are approximated by a plate model approximation (McKenzie, 1969) assuming a subduction velocity of 2 cm yr^{-1}.

Slabs are prescribed in the GWB along a line on the surface (trench). At this trench, it allows to describe the thickness and dip of the slab along a certain length. This can be done in one segment or several segments where the thickness and dip can linearly increase or decrease. In the case of the Aegean and Antalya slab, the GWB requires several segments to describe its geometry. This model holds a balance between a simple model geometry, common slab thicknesses and a degree of adherence to inherently uncertain tomography. To this end, all slab segments in this model start horizontally at 100 km thick and curve downwards to a certain dip, after which multiple other segments may be described (Figure 3.7). The angle and length of segments are informed by the local tomography, but the thickness is 100 km for all segment, increasing to 150 km thickness from the third curved segment onward where applicable. These sections are then laterally interpolated to construct a 3D model.

Figure 3.6 provides the overview of the used sections for the Aegean slab, which are then presented in Figure 3.8.

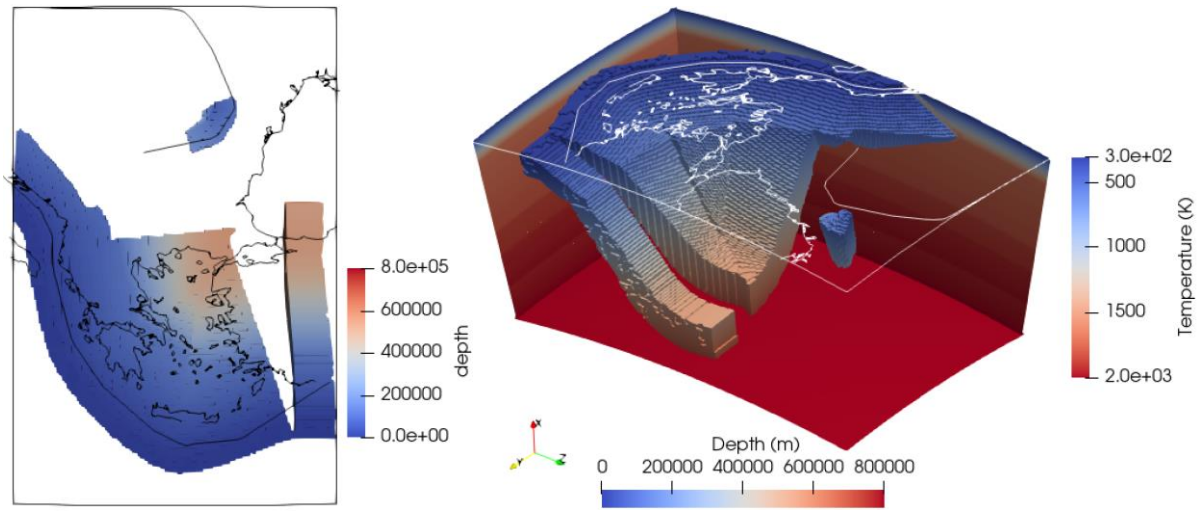

Figure 3.5 left: top view of the 3D slabs constructed using the GWB. Right: View from the NE to SW of the 3D model. Visible are the main Aegean slab, the Antalya slab segment, the shallow Dinarides slab attached to the Aegean slab and finally the separate Vrancea slab.

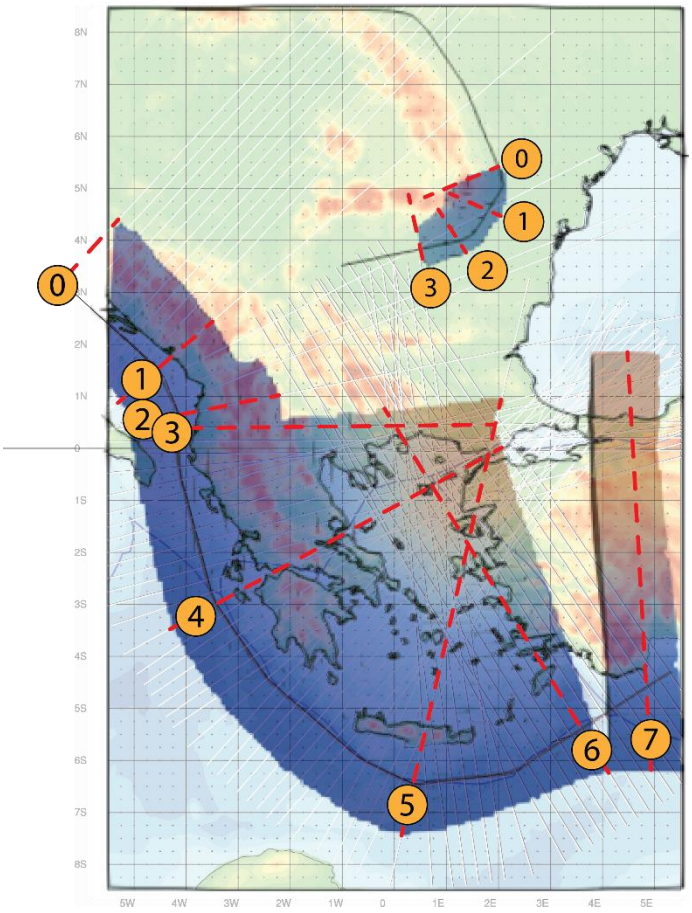

Figure 3.6 Map of the region and the 3D GWB model superposed on each other. Indicated in orange with red dashed line are the chosen sections used to construct the slab from the UU-P07 tomographic model (Figure 3.8). These are then laterally interpolated to the 3D model seen here.

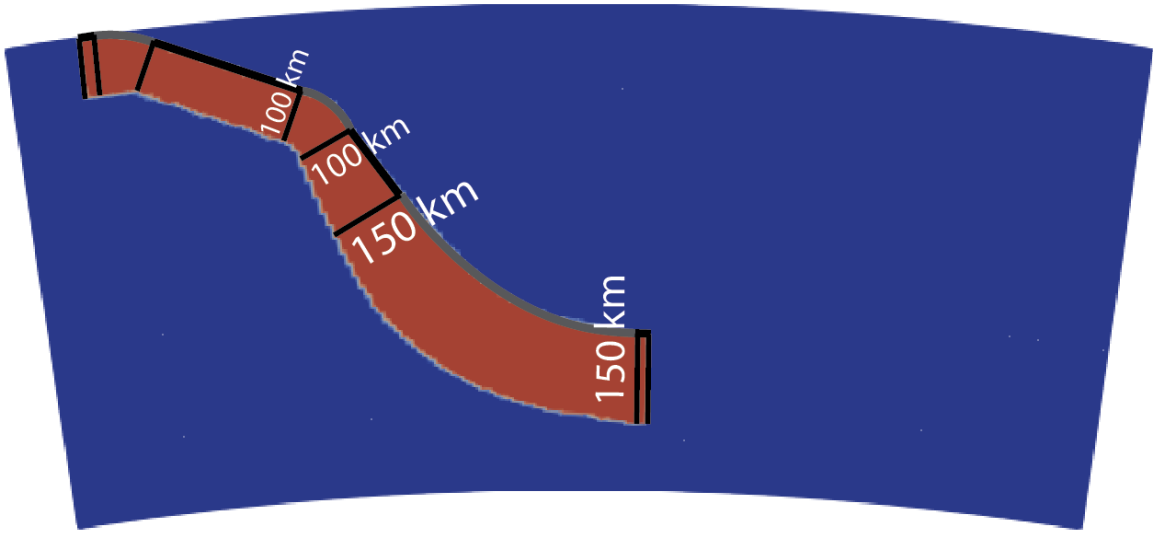

Figure 3.7 Typical geometry of a GWB section of the subducting slab, consisting of linear (black) or curved (grey) segments. Shallow segments are 100 km thick, increasing to a constant 150 km thickness from the third linear segment onward (where applicable).

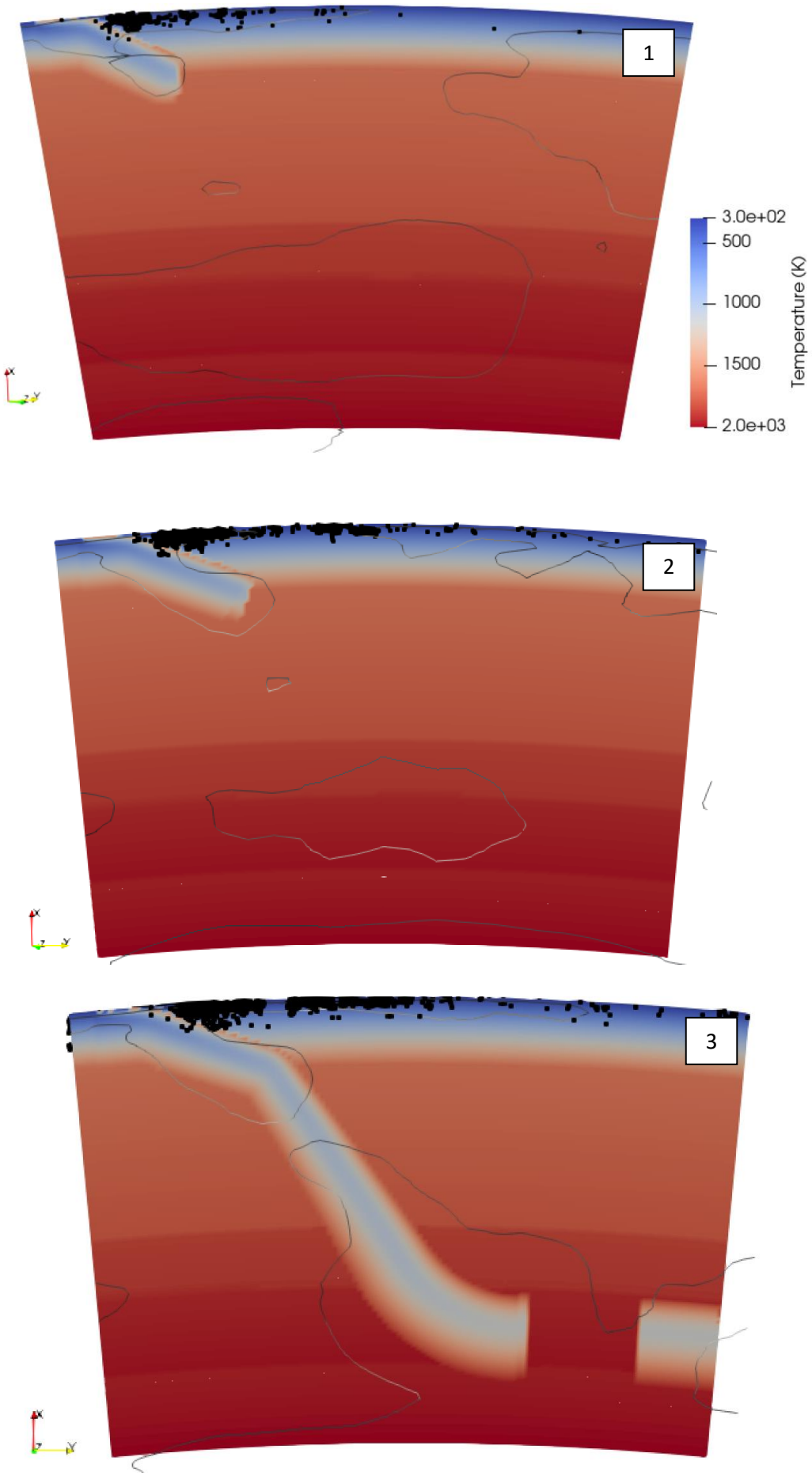
1
2
3
3.0e+02
500
1000
1500
2.0e+03
Temperature (K)

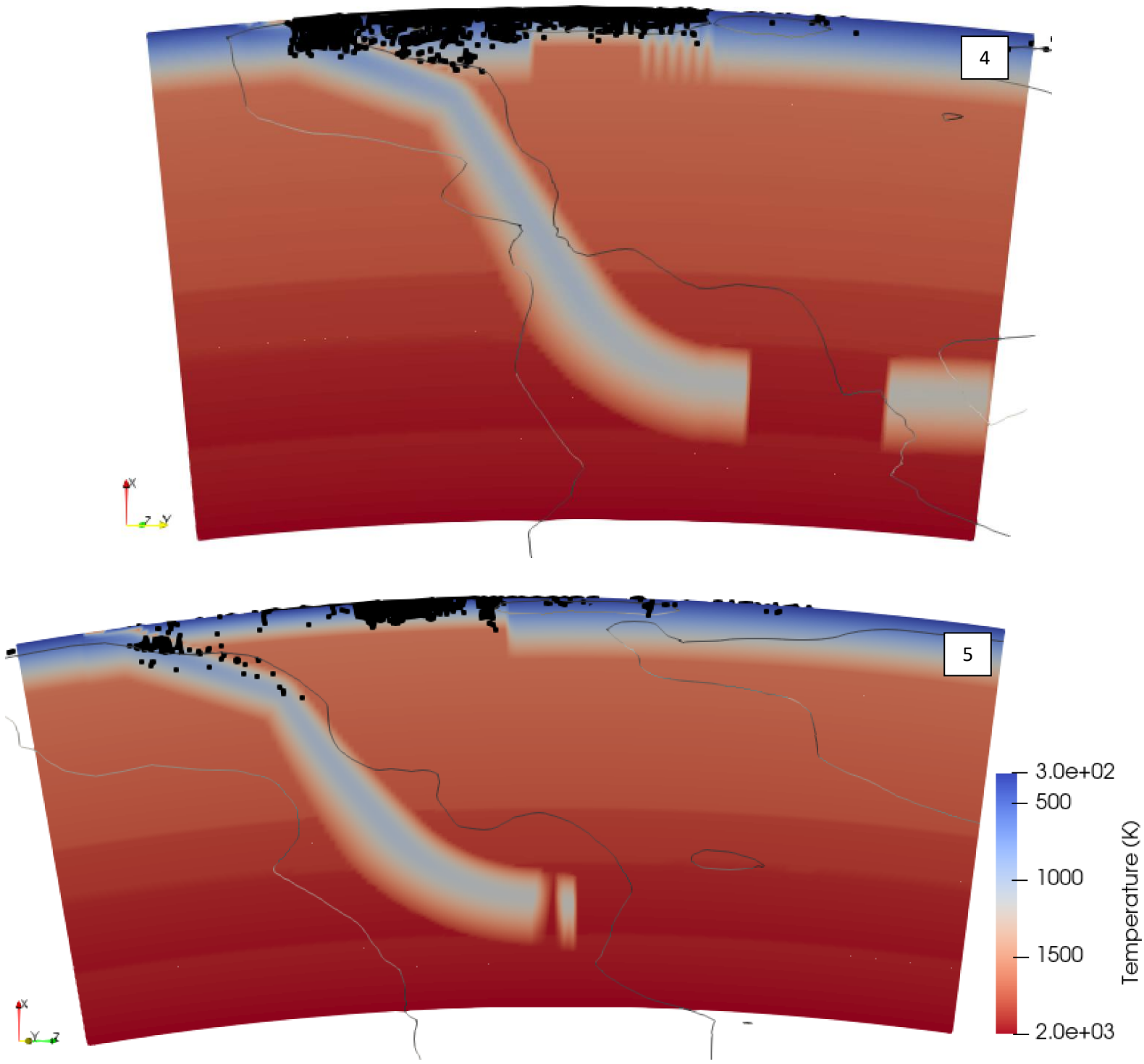
4
5
3.0e+02
500
1000
1500
2.0e+03
Temperature (K)

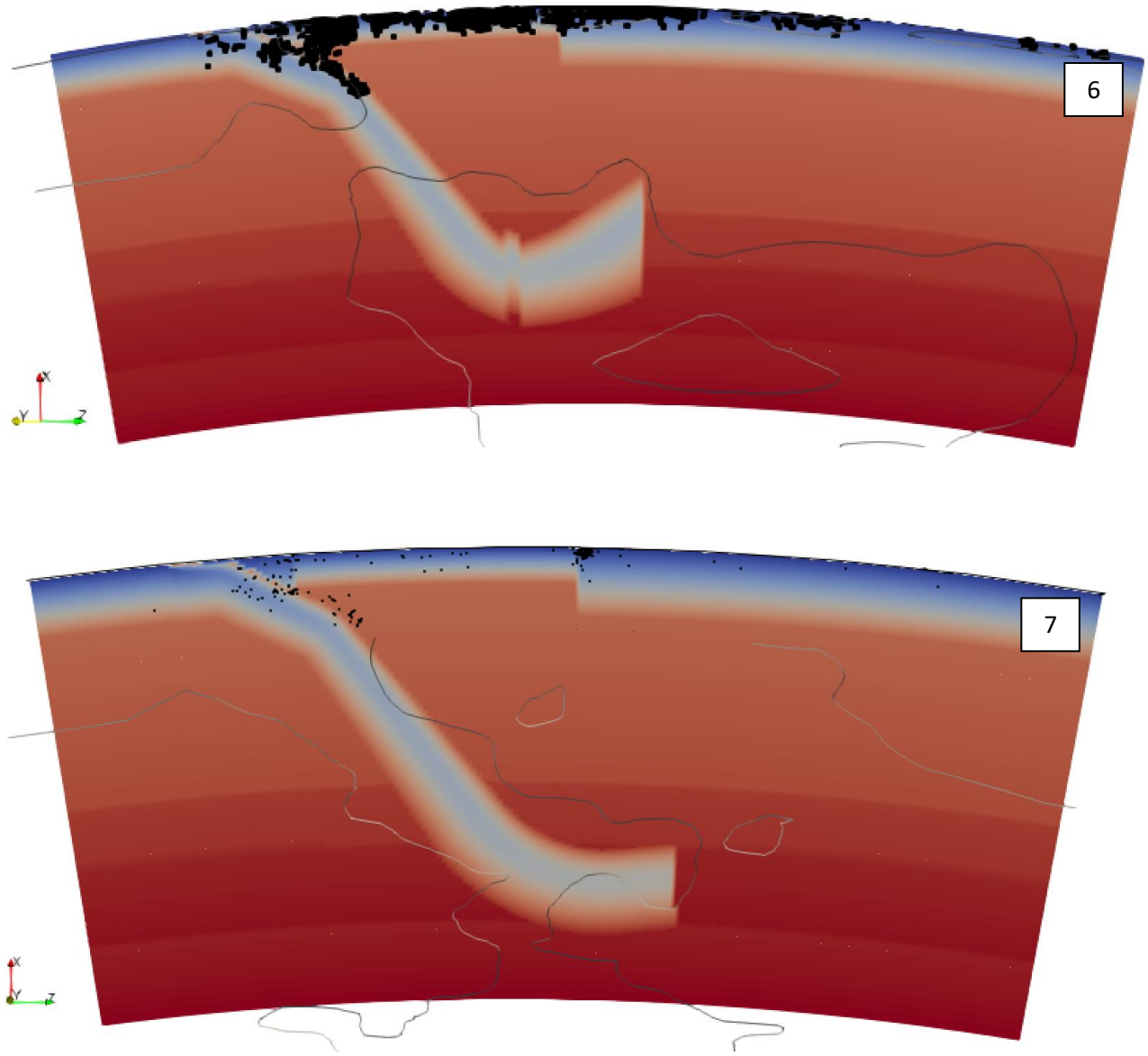

Figure 3.8 Sections of the Aegean slab, displaying the temperature distribution, the local earthquake hypocenters in black, and the used contour of the UU-P07 tomographic model.

Similar to the Aegean slab, the Vrancea slab was constructed by using four local tomographic slices. Its geometry is presented in Figure 3.9 which is comparable to the observed anomaly by Martin et al. (2006) (Figure 2.4). The slab encompasses the seismogenic NE segment and an aseismic deeper segment in the SW.

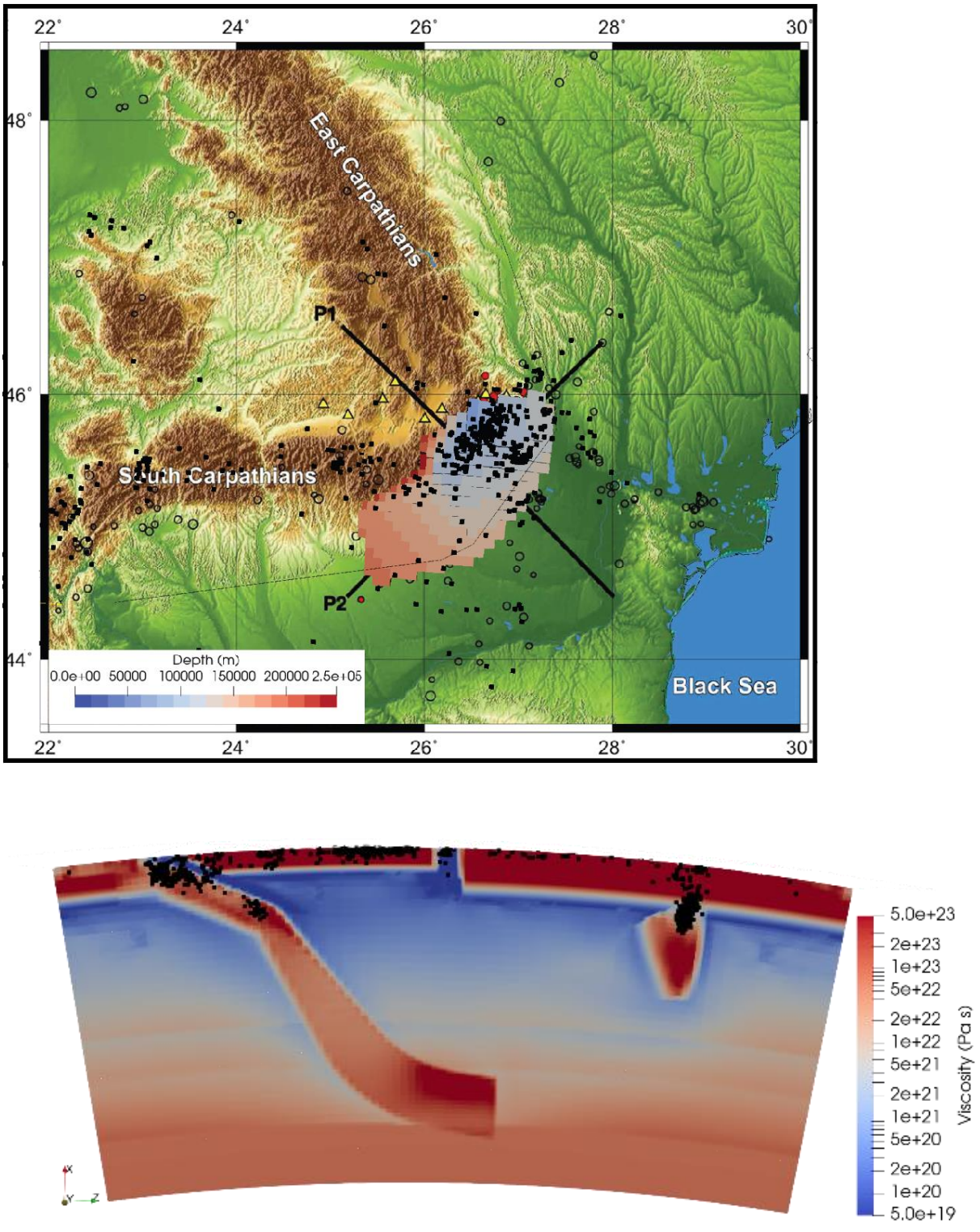

Figure 3.9 Top: map view of the Vrancea slab and earthquake hypocenters. Bottom: South-north cross section through the model displaying the Vrancea slab on the right. The Vrancea slab has a shallow seismogenic section in the NE and aseismic deep and detached section in the SW.

Initial temperature distribution

The initial model has a 1D temperature distribution (Figure 3.10), which is locally overwritten by the temperature field of slabs. The field increases in temperature linearly between the surface, LAB, and the 410, 520 and 660-discontinuities. The depth of the LAB is 120 km (Eurasia), 60 km (Aegean-Anatolia) and 100 km (Africa) where the temperature is set to 1682 K, 1650 K and 1672 K, respectively. These temperatures are taken from a recent study on the 410 km discontinuity temperature, where the temperature is extrapolated by assuming adiabatic behavior (Katsura, 2022).

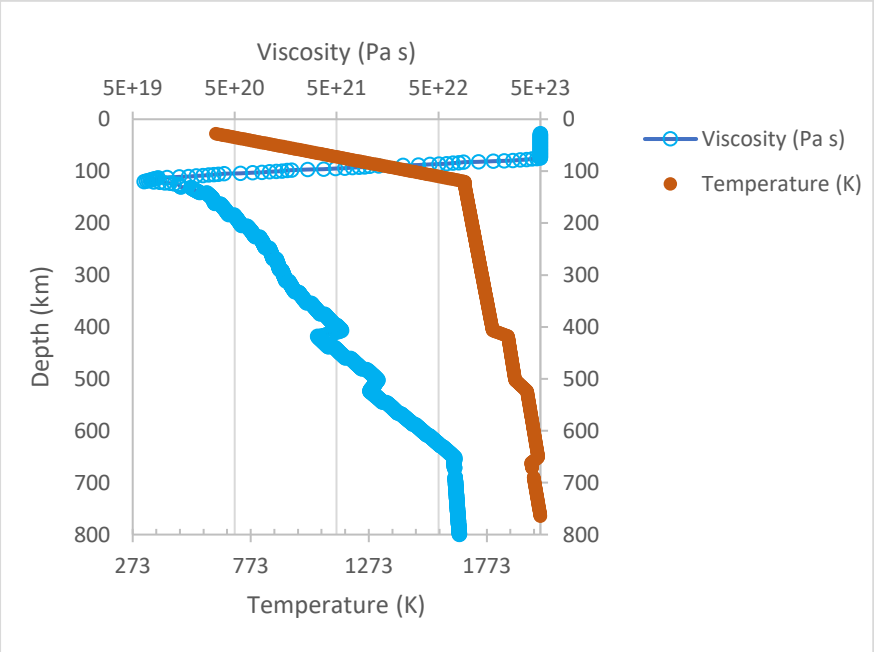

Figure 3.10 1D Temperature & viscosity distribution of the model.

Rheology & Material properties

The mechanical behavior of the model is prescribed by a visco-plastic rheology, which envelops dislocation and diffusion creep, and brittle-plastic failure. The viscosity following from diffusion and dislocation creep is described as:

$$\eta = \frac{1}{2} A^{-\frac{1}{n}} d^{\frac{m}{n}} \dot{\varepsilon}_{ii}^{\frac{1-n}{n}} \exp\left(\frac{E + pV}{RT}\right)$$

where η is viscosity, A is the diffusion/dislocation creep prefactor, d is the grain size, $\dot{\varepsilon}_{ii}$ is the second invariant of the strain rate tensor (in s^{-1}), E is the activation energy, p is pressure, V is activation volume, R is the gas constant and T is the temperature. m and n are constants, where m=2 or 3 and n=1 gives pure diffusion creep, and m=0 and n~3 describes power law creep by glide & climb of lattice dislocations. Plastic deformation in this model follows a Drucker-Prager formulation for the effective viscosity in 3D:

$$\eta_{\text{eff}}^{\text{pl}} = \frac{\sigma_y}{2\dot{\varepsilon}_{ii}} \qquad \sigma_y = \frac{6C\cos(\phi)}{\sqrt{3}(3 - \sin(\phi))} + \frac{6\sin(\phi)P}{\sqrt{3}(3 - \sin(\phi))}$$

Here, σ_y is the yield stress (in Pa), φ is the internal angle of friction (in degrees) and C is the material cohesion (in Pa). The effective viscosity is a harmonic average of the three deformation mechanisms. This amounts to the weakest deformation mechanism dominating the effective viscosity. Further material parameters used for all compositional fields are described in Table 1. A 1D viscosity profile is shown in Figure 3.10 for a region relatively undisturbed by large scale mantle flow. The model has a minimum and maximum viscosity cut-off at $5*10^{19}$ and $5*10^{23}$ Pa s. However this is merely indicative and not necessarily an exact plot for the majority of the domain.

Table 1 Material parameters used in this study. Creep parameters are based on Čížková et al. (2020) and tuned to a more viscous rheology considering Olivine flow laws from Hirth and Kohlstedt (2003) and personal communications with E. van der Wiel. Cohesion & angle of internal friction follow Glerum et al. (2021). As flow in the lower mantle is dominated by diffusion creep, the model uses a near-zero prefactor and arbitrary activation energy and volume for dislocation creep.

Parameter	Symbol	Unit	Slab	Upper Mantle	Lower Mantle	Lithosphere	Plate boundaries
Diffusion creep							
Prefactor	A_{diff}	$Pa^{-1}s^{-1}$	$7.0\cdot10^{-10}$	$7.0\cdot10^{-10}$	$1.0\cdot10^{-17}$	$7.0\cdot10^{-10}$	$7.0\cdot10^{-10}$
Activation energy	E_{diff}	$Jmol^{-1}$	$3.70\cdot10^{5}$	$3.70\cdot10^{5}$	$2.00\cdot10^{5}$	$3.35\cdot10^{5}$	$3.35\cdot10^{5}$
Activation volume	V_{diff}	$m^3\ mol^{-1}$	$6.4\cdot10^{-6}$	$6.4\cdot10^{-6}$	$1.1\cdot10^{-6}$	$1.1\cdot10^{-6}$	$4.8\cdot10^{-6}$
Grain size exponent	m	-	3				
Dislocation creep							
Prefactor	A_{disl}	$Pa^{-ndisl}s^{-1}$	$6.51\cdot10^{-16}$	$6.51\cdot10^{-16}$	$1.70\cdot10^{-170}$	$6.51\cdot10^{-16}$	$7.70\cdot10^{-39}$
Activation energy	E_{disl}	$Jmol^{-1}$	$5\cdot10^{5}$	$5\cdot10^{5}$	$5\cdot10^{5}$	$9\cdot10^{5}$	$9\cdot10^{5}$
Activation volume	V_{disl}	$m^3\ mol^{-1}$	$13\cdot10^{-6}$	$13\cdot10^{-6}$	$13\cdot10^{-6}$	$13\cdot10^{-6}$	$13\cdot10^{-6}$
Stress exponent	n	-	3				1
Cohesion	C	Pa	$5\cdot10^{7}$	$1\cdot10^{8}$	$1\cdot10^{8}$	$1\cdot10^{8}$	$1\cdot10^{6}$
Angle of friction	Φ	°	0	15	15	25	0
Other parameters							
Density	ρ	$kg\ m^{-3}$	3300	3300	4600	3200	3200
Heat capacity	C_p	$J\ kg^{-1}\ K^{-1}$	1250	1250	1250	1250	1250
Thermal conductivity	k	$W\ m^{-1}\ K^{-1}$	3	3	3	3	3
Thermal diffusivity	κ	$m^2\ s^{-1}$	$1\cdot10^{-6}$	$1\cdot10^{-6}$	$1\cdot10^{-6}$	$1\cdot10^{-6}$	$1\cdot10^{-6}$
Thermal expansivity	α	K^{-1}	$3.5\cdot10^{-5}$	$2.0\cdot10^{-5}$	$2.0\cdot10^{-5}$	$3.5\cdot10^{-5}$	$3.5\cdot10^{-5}$

Results

Pre-reference model

From the model setup described previously, numerous experiments were run to obtain a reference model. First improvement of the surface motion response was obtained by lowering the viscosity of the plate boundary fault and NAF to ~ $5*10^{19}$ Pa s. The temperature profile of the Aegean slab was tuned from a 5 cm yr^{-1} to 2 cm yr^{-1} plate model velocity to increase overall temperature and consequently decrease the overall viscosity of the slab. The Aegean slab is extended eastward with a segment attached to Africa but not to the rest of the slab. This segment corresponds to the Antalya slab which we attach to the African plate laterally to the Aegean and Cyprus slabs (Berk Biryol et al. 2011). This improved the flow across the plate boundary interface and the general rotation of Anatolia.

The overall viscosity during pre-reference model explorations was likely skewed to high values and possibly still is. The reason for this is purely practical: a more viscous model leads to lower model run time allowing for a higher frequency of experimental refinement. The experience from previous work (van Amerongen 2023, Guided Research) is that a more rigid model behaves more predictably for inexperienced modelers and novel model set-ups. Aegean slab viscosity, related to the roll-back of the Aegean region, was the central factor in finding the reference model which is presented next.

Reference model

Surface flow pattern

Figures 4.1a-d show the reference model predicted surface flow field and the observed surface flow field, in both a Eurasia fixed reference frame as in a Global Hotspot Mantle Reference Frame (GMHRF). The reference model reproduces the first order characteristic features of the region. The model reproduces the westward motion of Anatolia (in GMHRF) and rotation to a near trench-perpendicular orientation within the Aegean region. The motion of the peninsula Peloponnese in the south of Greece, coherent with the central Aegean, is reproduced. Lastly, the model fits the rigid northeast motion of Eurasia and Africa, both in the order of ~10 mm yr^{-1}.

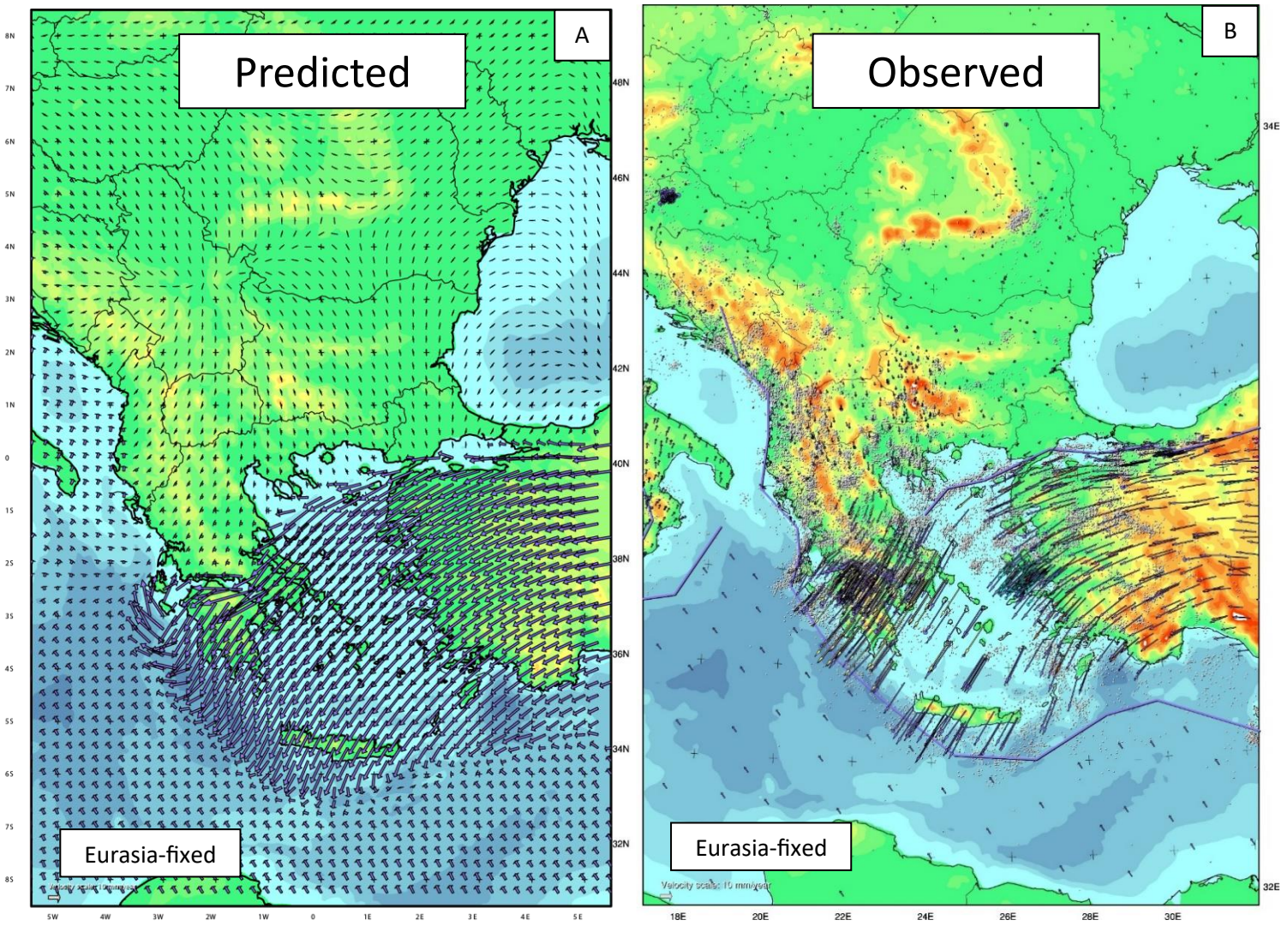
A
Predicted
Eurasia-fixed
B
Observed
Eurasia-fixed

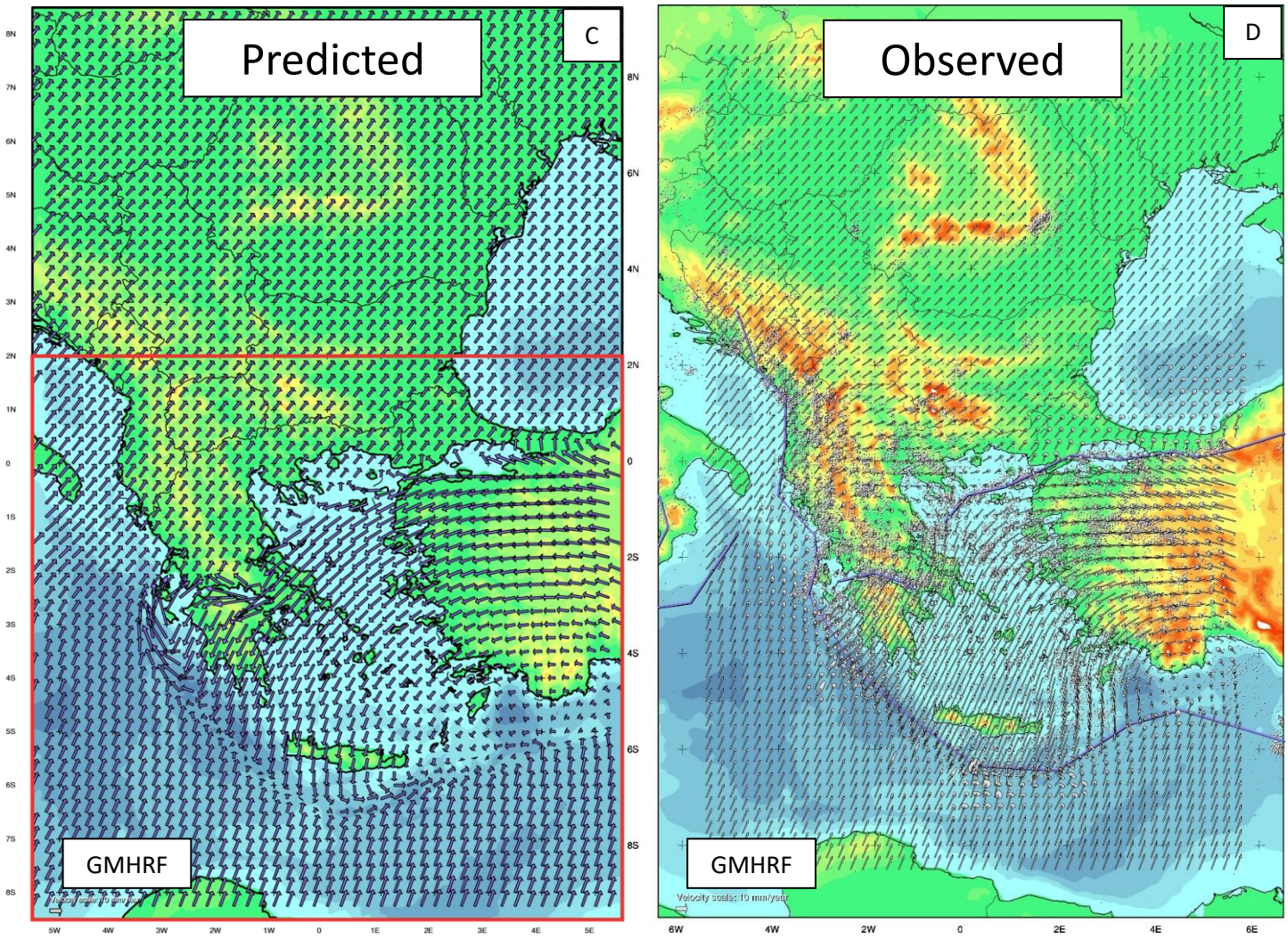

Figure 4.1 a) The predicted reference model surface flow field displayed in the Eurasia-fixed reference frame. Velocity scale is indicated in the bottom left (10 mm yr^{-1}). Boundary velocities are fixed. b) The observed GNSS surface flow field measured at GNSS stations. The plate velocity of Africa is visualized in the data-sparse Mediterranean Sea. c) The predicted reference model surface flow field in the GMHRF. The highlighted red box is the domain used in zoomed-in figures used later this chapter. d) The observed GNSS surface flow field in GMHRF, interpolated to a regular grid.

Differences between the reference model surface flow field and the observed flow field are spatially varying and can be subdivided in several regions (Figure 4.2). Misfit is lowest (0-5 mm/yr) in the Eurasian and African plates and Anatolia mainland. The misfit within the Aegean region is complex. In general, the velocity magnitude is low throughout, trending from low misfit (5-10 mm/yr) around Peloponnese, to medium misfit at and north of Crete (~10+ mm/yr) to high (~20 mm/yr) southeast of Crete on the plate interface. The orientation of misfit is trench-perpendicular from Peloponnese to Crete, and north-south directed along the west-coast of Turkiye up to Rhodes. Misfit is high and

of varying direction west of Peloponnese, through the Gulf of Corinth weak zone and northeast along the North Anatolian Fault.

A coherent misfit pattern is found on the mainland of Greece extending northward to North-Macedonia. The pattern shows a lack of southward velocity in the model and increasing misfit of magnitude further south. The orientation misfit here also shows a lack of a clockwise rotation in the area. Other misfits are mainly associated with the plate boundary zones of 30 km width.

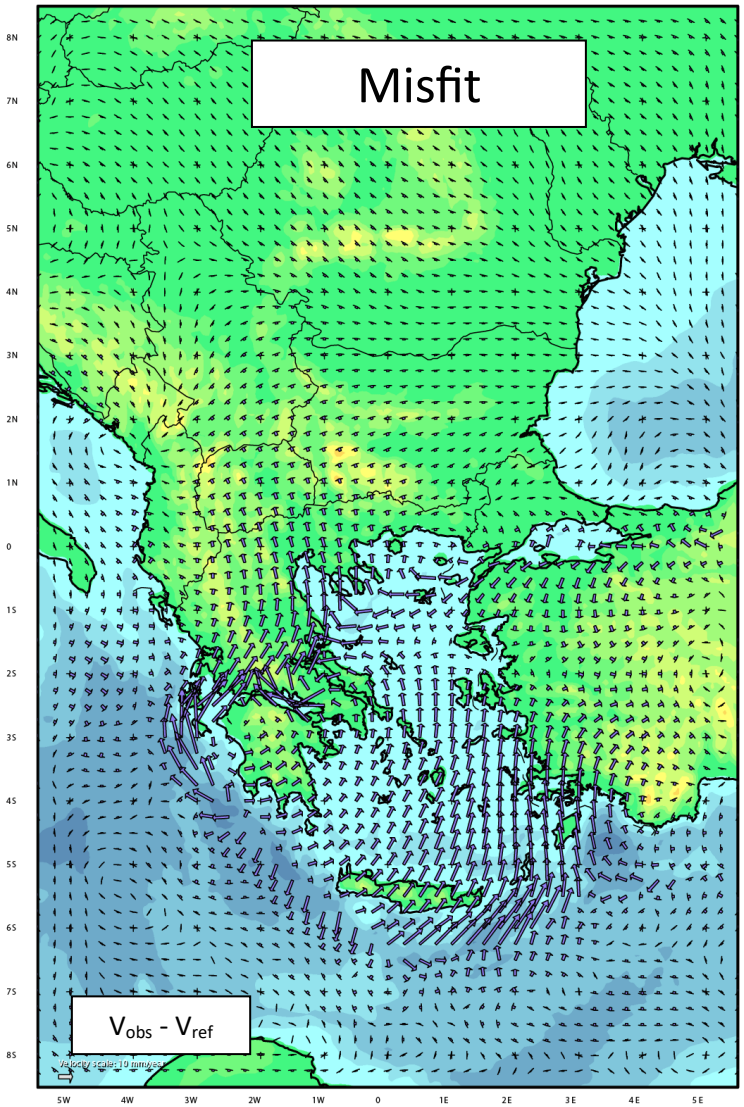

Figure 4.2 The difference between the observed GNSS surface flow field and the reference model surface flow field. Vectors opposing the observed direction of flow implies the reference model underpredicts the observed local velocity in amplitude.

Predicted vertical flow pattern

The north-south vertical flow profile predicted by our reference model is shown in Figure 4.3. Subduction and sinking of the Aegean slab is fastest in the top 300 km. Sinking is slowed in the lower section where the slab rests on top of the more viscous lower mantle. Viscous coupling of the slab to the surrounding mantle results in a similar flow pattern, albeit of lower magnitude. The Vrancea slab is modelled as mostly detached from the Eurasian plate. The slab displays some northward flow but is dominated by vertical sinking. The flow in the mantle is high in the low viscosity asthenosphere and highest in the mantle wedge. Overall velocity throughout the model decreases strongly with depth.

The vertical viscosity profile shows a coherent Eurasian and Anatolian lithosphere of $5*10^{23}$ Pa s. The viscosity of the Aegean slab varies from $5*10^{23}$ Pa s at the surface to $1*10^{23}$ Pa s at depth, increasing locally at its tip resting on the lower mantle. A higher strain rate is correlated to lowered viscosity as can be clearly seen in the Aegean slab at ~ 400 km depth, around the Aegean and Vrancea slabs at ~ 200 km depth, in the mantle wedge (note that mantle flow velocity is high in the invisible lateral direction) and through the two prescribed weak zones (Plate boundary fault and the NAF transform fault, clearly visible as zones of high strain rate in Figure 4.4).

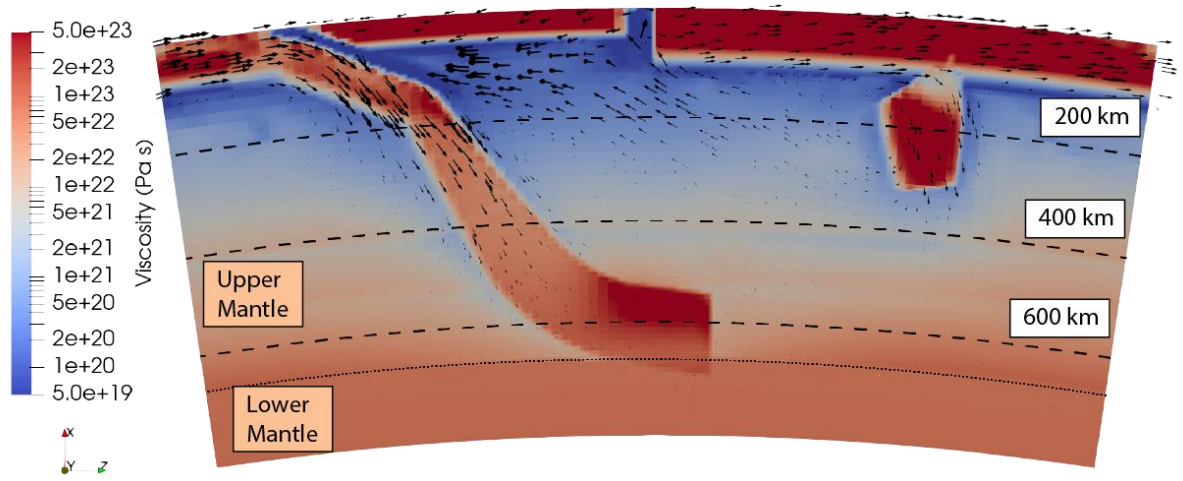

Figure 4.3 A 2D south-north cross section of the Aegean slab subducting beneath Anatolia and Eurasia. Velocity vectors are shown in black (vectors at the trench and within Eurasia are ~ 14 mm yr^{-1} and 9 mm yr^{-1} respectively). The background shows the viscosity profile in blue-red. Dashed lines are shown at 200 km, 400 km and 600 km depth, through which horizontal cross sections are made (Figure 4.5-4.8).

The viscosity in this model is the harmonic average of three deformation mechanisms - diffusion creep, dislocation creep and plastic yielding – of which the latter two are strain-rate dependent. Comparisons can be drawn to previous subduction modelling (Garel et al., 2014) to better understand the viscosity field. Plastic yielding is the dominant

deformation mechanism at shallow depth and low temperatures, here seen in the locally low viscosity and higher strain rate in the slab bend. Dislocation creep is dominant in the upper mantle under high strain rates, mostly visible here in the disturbed mantle surrounding the subducting slabs. Diffusion creep is dominant in the lower mantle and in the undisturbed upper mantle, seen here at the north and south edge of the profile with relatively low strain rates and high viscosity.

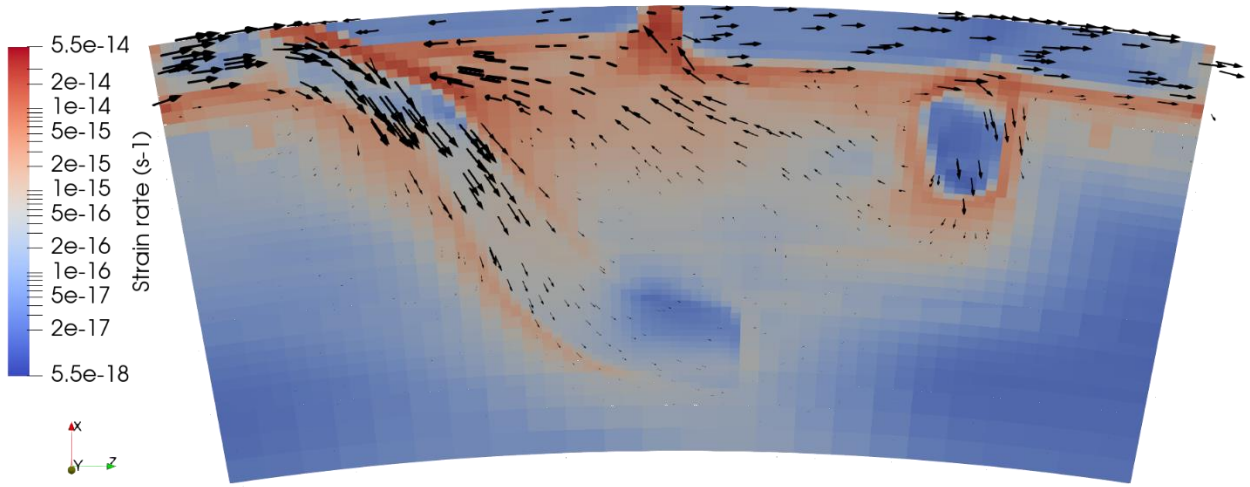

Figure 4.4 The 2D south-north cross section shown in Figure 4.3, through the Aegean slab subducting beneath Anatolia and Eurasia. The background shows the strain rate.

Predicted horizontal mantle flow pattern

200 km depth flow pattern

The prediction of the mantle flow field at 200 km depth (Figure 4.5 and 4.6) shows a dominant flow towards the center of the sinking Aegean slab. As the slabs sinks, the vertical sinking component of this diagonal interface creates a low pressure region in front of the slab. Ambient mantle is also pushed away from behind the slab and flowing around the edges of the slab. In Figure 4.6 it is visible how the sub-slab mantle is viscously coupled to the slab and dragged NE and downwards into the mantle. At this depth it is also seen that flow from the Aegean slab edge impinges on the front side of the Vrancea slab, which could be correlated to its anomalous verticality. Finally, Figure 4.6 shows the vertical sinking of the Vrancea slab into the mantle.

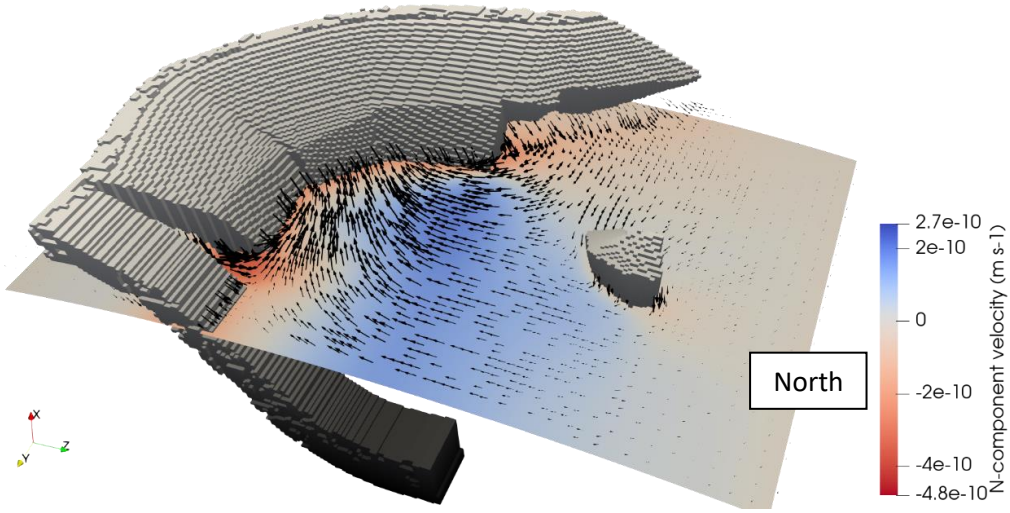

Figure 4.5 3D model of the subducting slabs colored in white to black. A cross section is given at 200 km. The velocity vectors are shown for the flow of the slabs and of the surrounding mantle. The magnitude of N-S flow is shown in blue (north) to red (south).

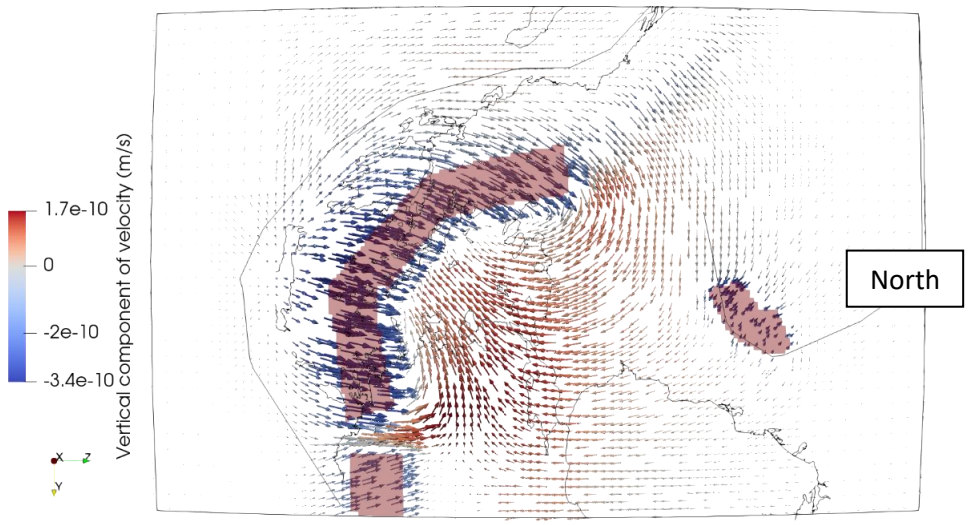

Figure 4.6 A map-view slice of the 3D velocity field at 200 km depth, identical to figure 4.4. Red areas show the location of the Aegean, Antalya and Vrancea slabs at these depths. Vector size is equal to Figure 4.5.

400 km depth

Figure 4.7 and 4.8 show the mantle flow field at 400 km depth (note the 3x+ scale difference. General velocity is lower and should be compared via the vertical cross section Figure 4.3). This depth is below the mantle wedge and is characterized not by a dominant flow into the Aegean slab center, but by a general 'push' of mantle material away from the slab. Flow north of the Aegean slab converges locally to below the Bosporus Strait, where it flows upward to fill the void left by the material flowing into the mantle wedge (Figure 4.5 & 4.6). Flow south of the slab is low in magnitude and diverging. Below west Greece the flow is generally NW, coupled to the Aegean slab.

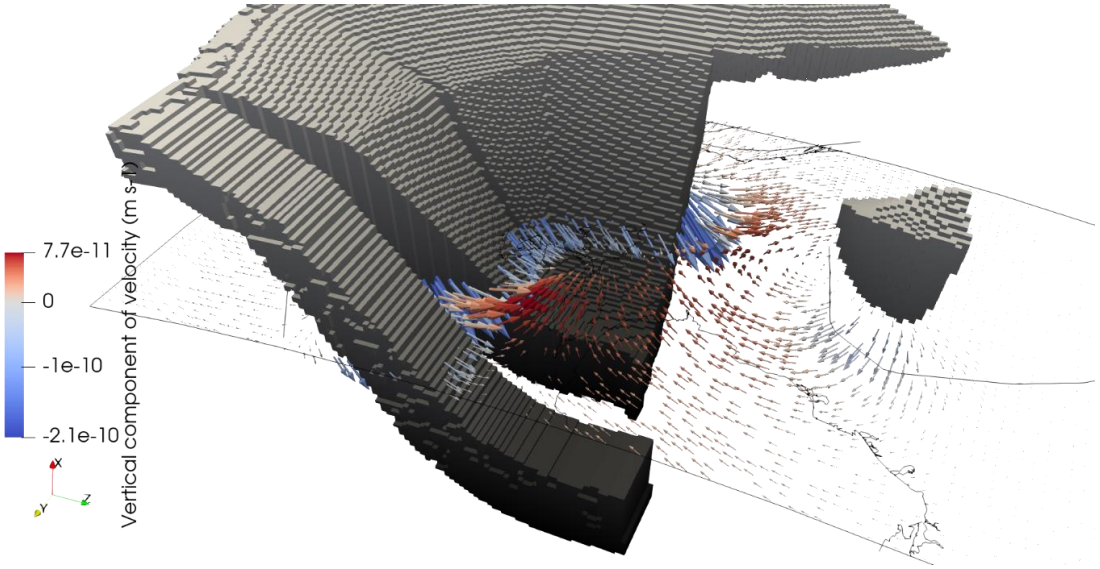

Figure 4.7 3D model of the subducting slabs colored in white to black. A cross section is given at 400 km. The 3D velocity vectors are shown for the flow of the slabs and of the surrounding mantle. The magnitude of vertical flow is shown in red (up) to blue (down). The relative vector scale 333% larger than Figure 4.5 & 4.6.

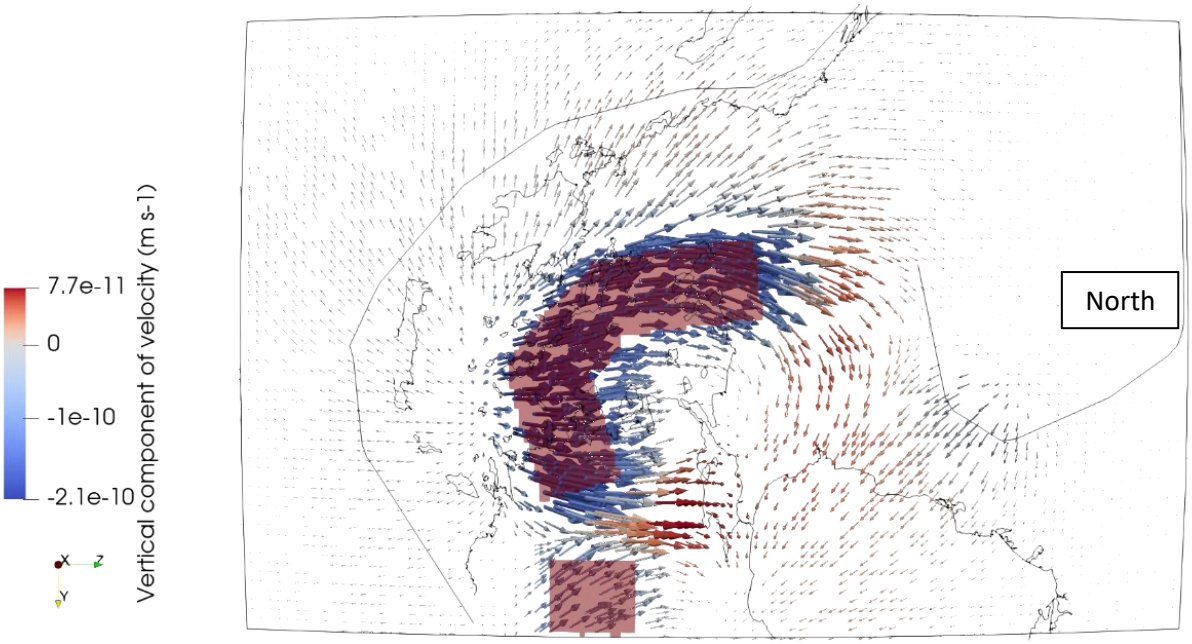

Figure 4.8 A map-view slice of the velocity field at 400 km depth, identical to figure 4.4. Red areas show the location of the Aegean and Antalya slabs at these depths. The relative vector scale 333% larger than Figure 4.5 & 4.6.

600 km depth

Figures 4.8 and 4.9 show how flow velocity is much lower at 600 km depth and is simple in direction. Only the Aegean slab propagates significant flow in a direction (northeast). Flow surrounding the slab is generally diverging and of lower magnitude than at shallower depths. Flow in and around the slab is downward, flow in the ambient mantle is upward.

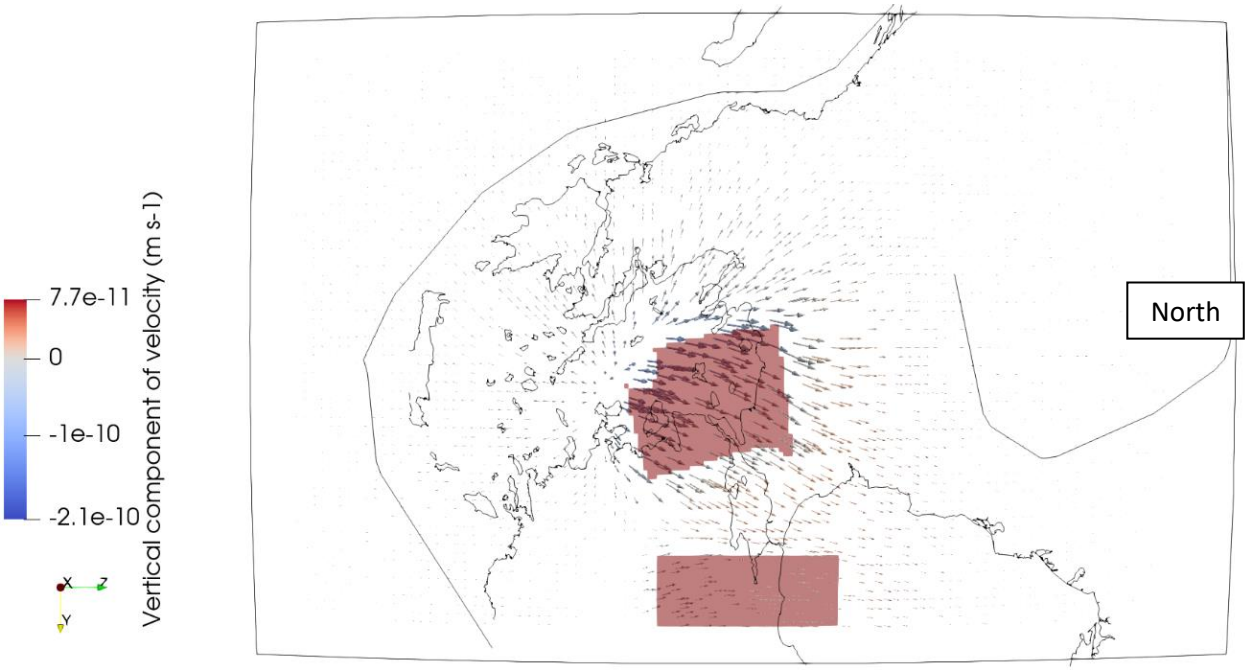

Figure 4.9 A map-view slice of the velocity field at 200 km depth, identical to figure 4.4. Red areas show the location of the Aegean and Antalya slabs at these depths. The relative vector scale 333% larger than Figure 4.5 & 4.6.

Reference model sensitivities

Increased coupling of Vrancea slab

Figures 4.10 and 4.11 demonstrate a model with a Vrancea slab, is attached to the Eurasian plate. The Vrancea slab has a higher NE-velocity as it is now attached to the overriding Eurasian plate. This implies that the slab is being pulled/dragged through the surrounding mantle, increasing the compressive stresses on the slab.

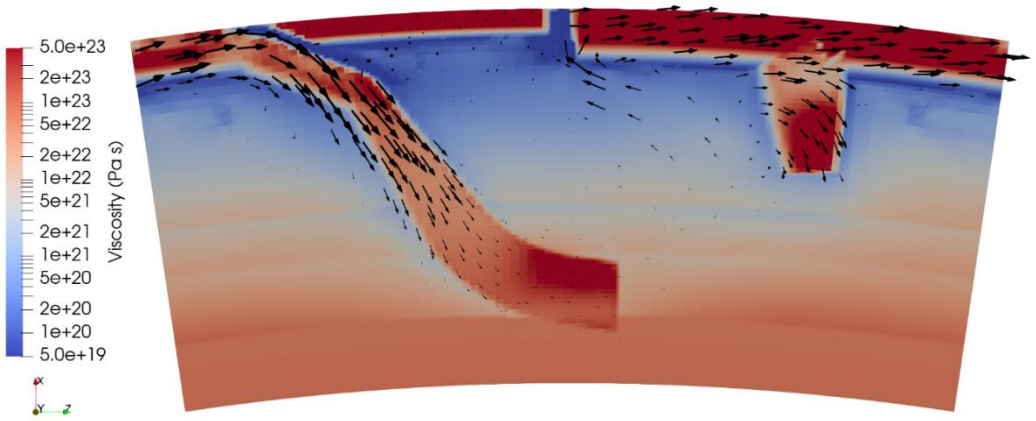

Figure 4.10 The 2D south-north cross section of the Aegean slab subducting beneath Anatolia and Eurasia also shown in Figure 4.3, for a Vrancea slab attached to the Eurasian plate. Velocity vectors are shown in black (vectors at the trench and within Eurasia are ~ 14 mm/yr and 9 mm/yr respectively). The background shows the viscosity profile in blue-red.

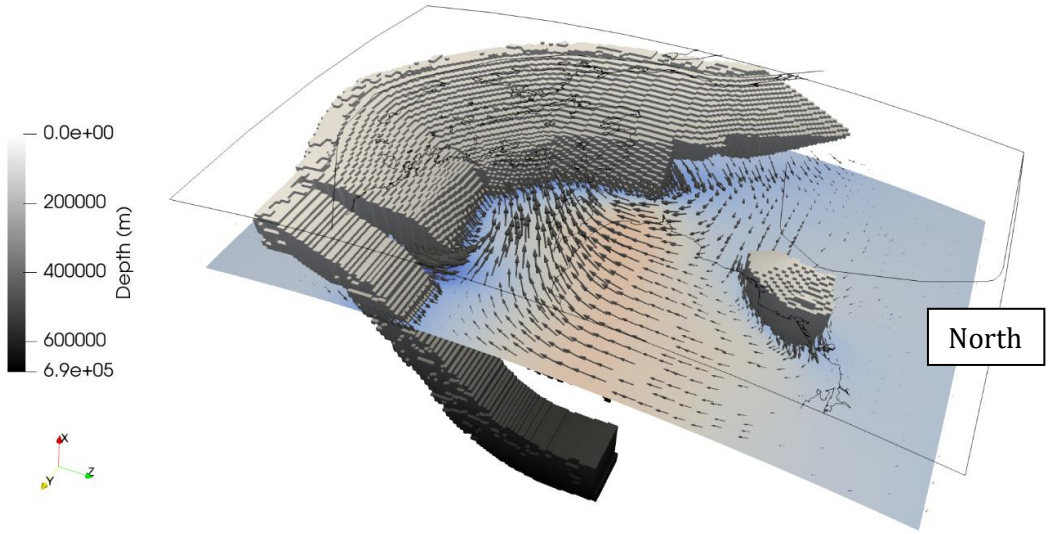

Figure 4.11 3D model of the subducting slabs colored in white to black. A cross section is given at 200 km. The velocity vectors are shown for the flow of the slabs and of the surrounding mantle. The magnitude of N-S flow is shown in blue (north) to red (south). The relative vector scale is 100%, equal to Figure 4.5 & 4.6.

Removing the Aegean slab

Figure 4.12 shows the resulting surface flow fields for experiments where the Aegean and Antalya slab were removed. The model yields two distinctly different interpretations, depending on the choice of reference frame.

In a Eurasia fixed reference frame (Figure 4.12a), the characteristic westward motion of Aegean - Anatolia is present even without the Aegean slab, which is a commonly hypothesized main driver of the region. Visualizing the result in a mantle reference frame(Figure 4.12b), however, shows a pure westward motion of Anatolia with no S-component and a more gradual turn SW. This displays that the Euler pole rotation between Eurasia and Africa in a Eurasia-fixed reference frame adds an apparent S-component to the Aegean flow field. This emphasizes that the roll-back in the Aegean region should be viewed in a mantle reference frame. The misfit of the velocity field (4.12c) further shows that the impact of the slab on the flow field is S-oriented nearly everywhere in the Aegean region. At and east of Crete the surface flow shows that the decrease in motion is not S- but SE-oriented, which could be related to its proximity to the east margin of the slab and its local impact on roll-back.

The predicted westward motion of Anatolia and minute rotation in the Aegean are explained in context of the boundary conditions in Anatolia. The prescribed kinematic boundary conditions in the reference model are the local expression of, in part, the slab pull driving its westward flow. In the absence of this pull, the boundary conditions now act as an external force pushing Anatolia westward. The rest of the microplate accommodates this movement. In this area, the NAF weak zone is backed by the strong Eurasian lithosphere. The Anatolia plate cannot indent or deform the Eurasian plate and is deflected along the NAF in a WSW orientation as can be seen in the predicted flow field.

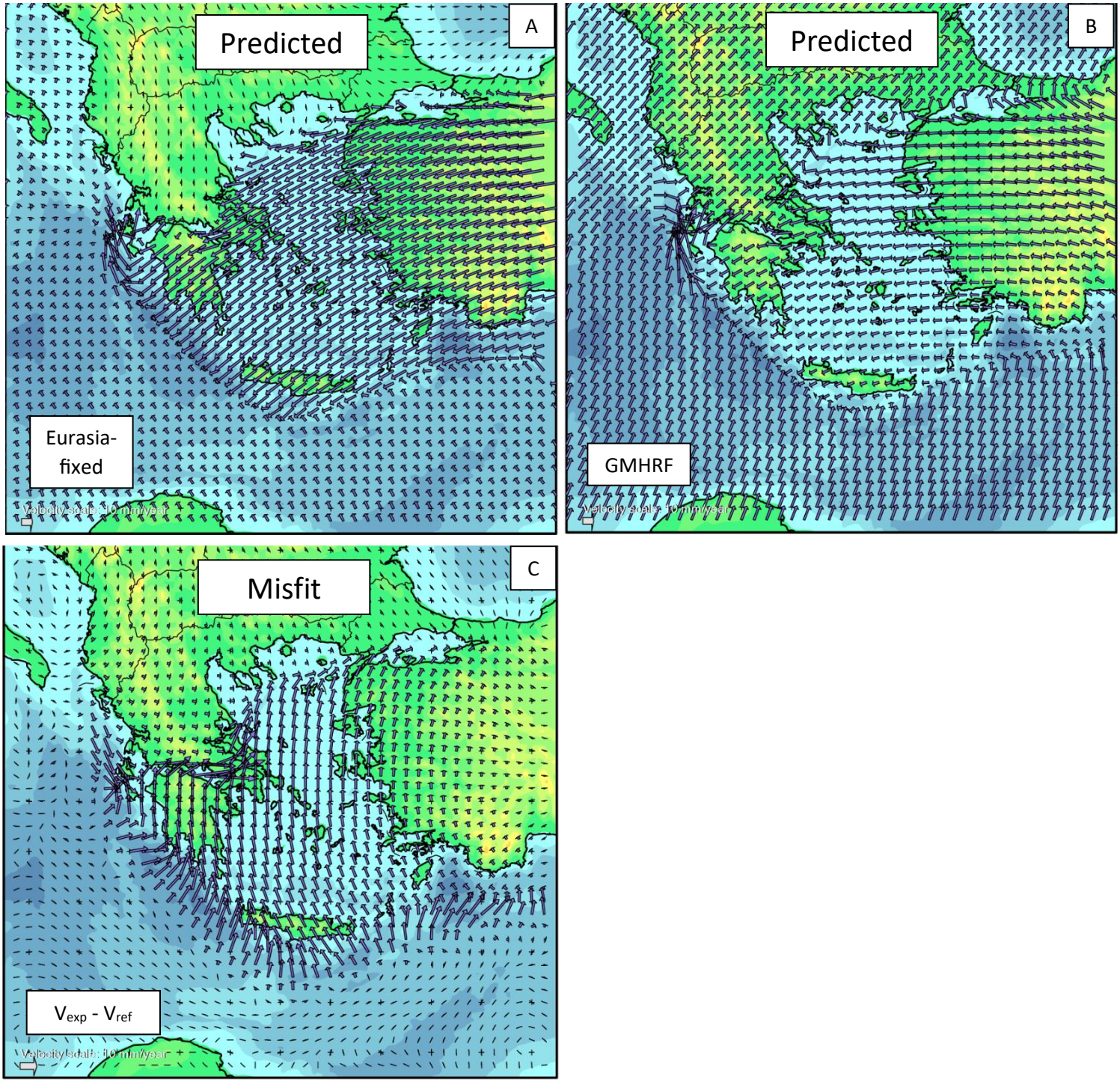

Figure 4.12a-c a) Predicted surface flow field in a Eurasia fixed reference frame. b) Predicted surface flow field in GMHRF c) Difference between the reference model and No slab experiment.

Plate boundary viscosity versus slab viscosity

Figure 4.13 (to be used with Table 1) demonstrates the effect that slab viscosity and plate boundary viscosity have on the reference model. 4.13b shows that an increase in plate boundary viscosity from $5*10^{19}$ Pa s to 10^{20} Pa s creates a reduction in the Aegean - Anatolia plate velocity in the order of several mms yr^{-1}. The azimuth of the reduced velocity is NW on Peloponnese and the south Aegean, and N in the north Aegean. We explain this as a redistribution of lithosphere material to the west of the domain, as the south margin resists the incoming flow from the north.

This effect is compared to the weak slab experiment Figure 4.13c. In this experiment, the plastic cohesion of the Aegean slab is lowered from $5 * 10^7$ to $2 * 10^7$ Pa s, which reduces the viscosity of the Aegean slab from $5*10^{22}$ – $5*10^{23}$ Pa s to $5*10^{21}$ – $2*10^{22}$ Pa s. This increases surface flow by ~ 7 mm yr^{-1} in the Aegean region, oriented S and SSE east of Crete. The combination of these two effects is shown in Figure 4.13d. The flow field is still increased southward relative to the reference model but tempered in magnitude to 2-5 mm yr^{-1}.

The effect of the weakened slab experiment is not unexpected if it is regarded as the opposite of the 'no slab' experiment displayed in the previous chapter. The viscosity decrease of the slab increases its vertical sinking potential as its rigidity is reduced and flexing of the hinge is easier. This vertical sinking of a dipping slab translates to the trench as a trench-retreat, facilitating roll-back of the Aegean region and therefore increased southward velocity. The difference in orientation along the trench, exemplified in the SE-oriented retreat east of Crete, indicates that this phenomenon could be dependent on the local slab geometry and not of the regional trend (S to SW-ward).

However, the lack of SW-oriented roll-back west of Crete is not in line with this interpretation. A possible cause for this could be in the rigidity of Aegean - Anatolia. At $5*10^{23}$ Pa s, the viscosity of the microplate could be considered high for lithosphere that has underwent high levels of extension (Jolivet et al. 2013). A rigid Aegean - Anatolia plate in this geometrical setup could advance westwards and 'collide' with the Eurasian continent, rotating counter-clockwise along the SW bend of the NAF. The next set of experiments investigate this effect of Aegean - Anatolia viscosity.

Table 4.1 Overview of the experiments conducted with relation to slab cohesion and plate boundary cohesion.

	Plate boundary plastic cohesion (Pa) (1e24 anatolia)	
Slab plastic cohesion (Pa)	1.00E+06	2.50E+06
5.00E+07	Reference	I
2.00E+07	II	III

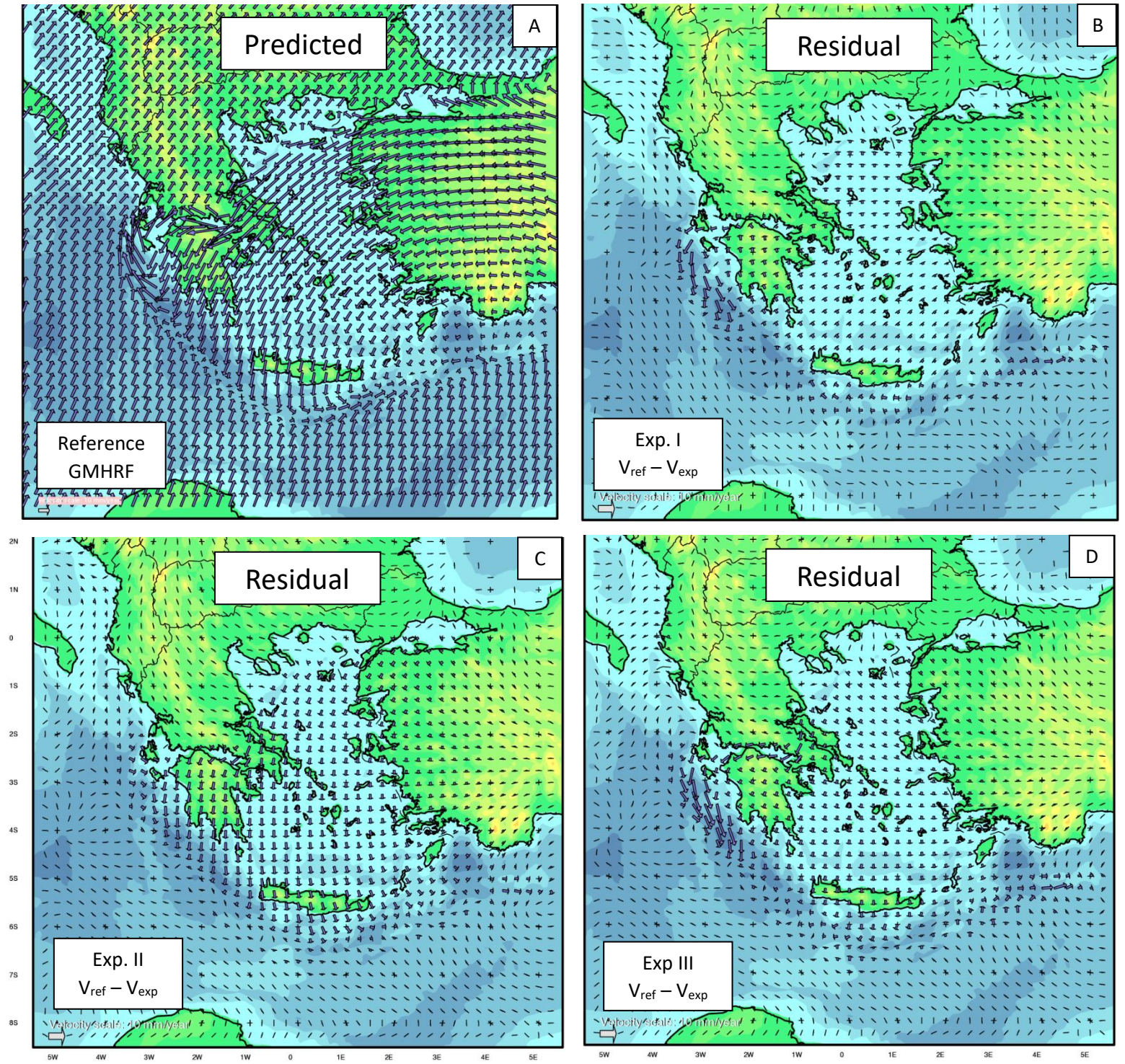

Figure 4.13 a) Reference model surface flow field (GMHRF) b) Difference (residual) field between the reference model and experiment I (table 4.1) c) experiment II d) experiment III.

Sensitivity to Anatolia & Aegean plate viscosity

Table 4.2 Overview of the experiments conducted with relation to the Aegean - Anatolia plate viscosity.

	Aegean - Anatolia plastic cohesion (Pa)		
Aeg-Ana angle of friction (°)	3.E+07	5.E+07	1.E+08
0 degrees	1e23 Pa s (IV)	1e23+ Pa s	5e23 Pa s
15 degrees	5e23 Pa s	5e23 Pa s	5e23 Pa s
25 degrees	5e23 Pa s	5e23 Pa s	5e23 Pa s (Ref)

The parameterisation of the model is complex and reductions in viscosity are a strongly nonlinear response to small changes in the prescribed material parameters. The section of the slab most relevant for roll-back is in its hinge and shallow (<150 km) domain (Holt, Becker & Buffett 2015), where plastic deformation is the dominant deformation mechanism (Garel et al. 2014). Therefore nine experiments were conducted on the material parameters relevant for plastic deformation, namely the internal angle of friction and the material cohesion (Table 4.2), and two end-members were found. The reference model lies in the higher-viscosity end-member and only a single tested model lies in the lower-viscosity end-member. This lower viscosity end-member is compared to the reference model in Figure 4.14a-c.

Differences between the reference model and the experiment are mostly confined to the Aegean region, and can be distinguished as a rotation regime (reference) or 'free flow' regime (weak Aeg – Ana). The orientation of the flow field in the weak Aeg – Ana experiment is near trench-perpendicular in the central Aegean region and around Crete (Figure 4.14b). Flow changes direction from SW to W on Peloponnese, following the flow pattern at the plate boundary and Gulf of Corinth weak zones. The flow east of Crete is undisturbed by the adjacent trench and also is largely oriented toward the SW trench.

The experiment does not predict the same strong southward flow around Crete and Rhodes, nor the coherent motion of Peloponnese. Figure 4.14c shows that the velocity field of the low Aegean - Anatolia viscosity experiment is enhanced by ~ 5 mm yr^{-1} in the W-direction at Rhodes and east Crete, and NW in the rest of the Aegean, Peloponesse and west Anatolia. Figure 4.14d illustrates that this model correctly predicts the magnitude of the E-W component of flow in the Aegean and SW Anatolia. The magnitude of the S-component of flow is too low in this model by ~ 10 mm yr^{-1}.

This experiment demonstrates that a lower Aegean - Anatolia plate viscosity enhances W flow of the Aegean region (via faster westward flow) and NW on Peloponnese (via faster westward flow, and reduced southward flow as its coherency to the Aegean is reduced). A higher viscosity shows more rigid rotation, with Peloponnese showing the same trend as central Aegean and the clear rotation along the south of Anatolia and east of Crete. Using the results from this experiment, and the knowledge from the previous experiment that a weaker slab enhances southward flow of the overriding plate, a new experiment is constructed where these parameters (overriding plate viscosity and slab viscosity) are combined.

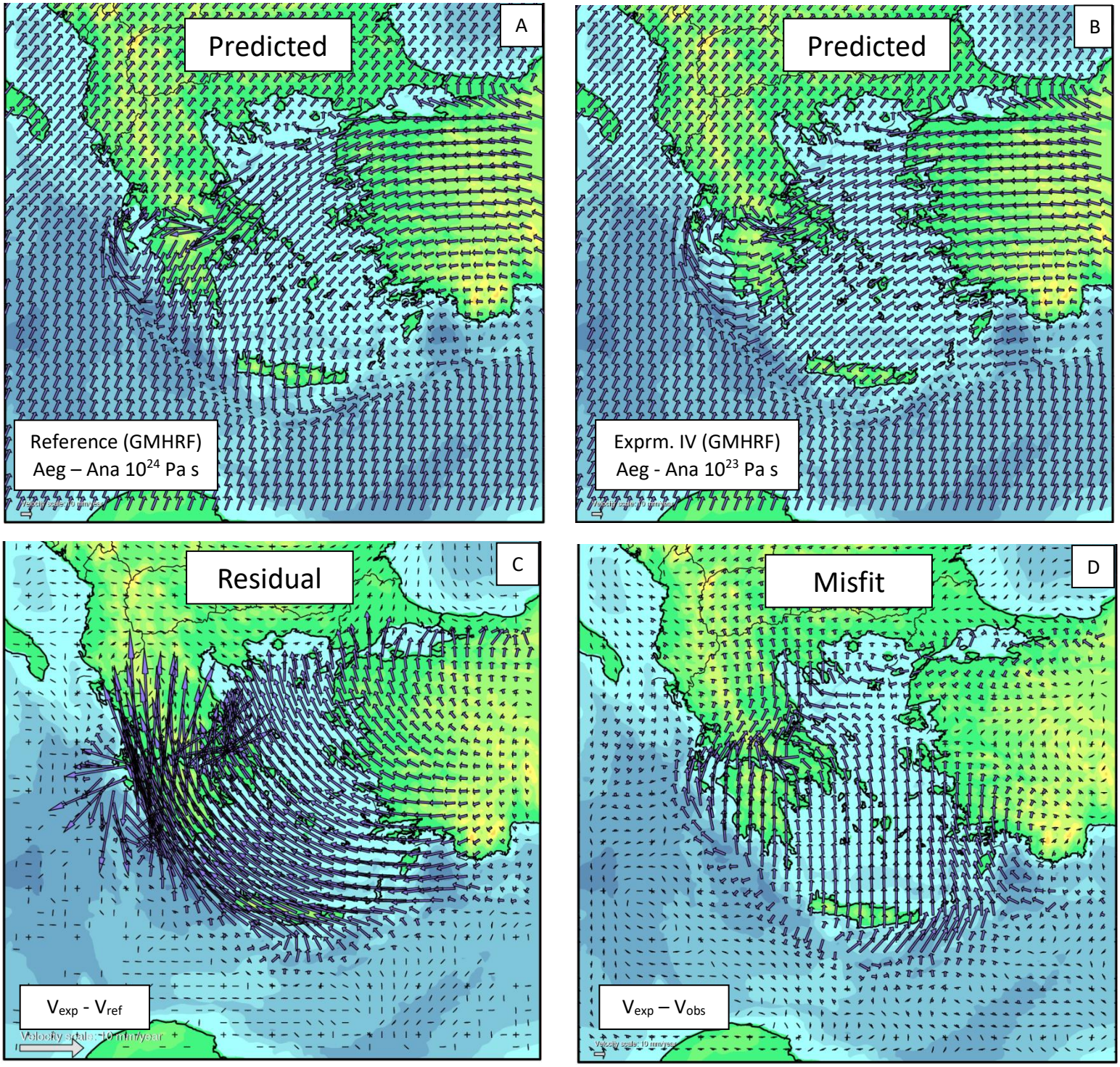

Figure 4.14 a) Reference model surface flow field (GMHRF) b) Experiment IV predicted surface flow field (GMHRF) c) Difference between the reference model and experiment IV (note the change in scale.) d) Difference between the reference model and the observed GNSS flow field.

Anatolia & Aegean viscosity versus slab viscosity

The experiments from previous chapter were expanded to investigate the sensitivity of a lower slab viscosity in relation to the overriding plate viscosity (Table 4.3).

Table 4.3 Overview of the experiments conducted with relation to slab viscosity and plate boundary viscosity.

Slab cohesion (Pa)	1e23 Pa s Ana/Aeg viscosity	1e24 Pa s Ana/Aeg viscosity
5.00E+07	IV	Reference model
2.00E+07	V	II

Experiments were conducted on the sensitivity of the reference model to the Aegean - Anatolia microplate viscosity vs. slab viscosity (Figure 4.15). The overall velocity in both models is increased by 5-10 mm yr^{-1} which is almost a doubling (Figure 4.15a-b). The orientation of the velocity field for both experiments show several different areas with a good and poor fit to the observed field (Figure 4.1d).

Experiment V (Figure 4.15a) shows an azimuth of the velocity field in the Aegean region which is antiparallel to the African plate velocity field, a feature recognized in the observed GNSS field for the west (Figure 4.1d). This orientation is mismatched on Peloponnese, where the field is rotated clockwise to a W-direction, and south of Crete, where the distinct S-direction is not reproduced. Experiment II (Figure 4.15b) reproduces the rigid SW movement of Peloponnese and S-direction of the region east of Crete but overestimates the clockwise rotation of the field within the Aegean region.

The differences in modelled flow field between the experiments and the reference model are shown in Figure 4.15c-d. The effect of a weaker slab on the reference model (Experiment II, Figure 4.15d) is also described in Figure 4.13c. In general, the weaker slab results in stronger southward motion of the overriding plate, per consequence of the geometrical gap created when the dipping slab sinks faster in the mantle. This applies for both the high and low Aegean - Anatolia plate viscosity.

The combined effect of both a lower Aegean - Anatolia plate viscosity and slab viscosity results in a model with an added 3-5 mm yr^{-1} S-directed flow component and a 3-7 mm yr^{-1} W-directed flow component. This is in first order interpreted to result from an increase in slab-pull and rollback, and the higher mobility of the overriding Aegean - Anatolia plate.

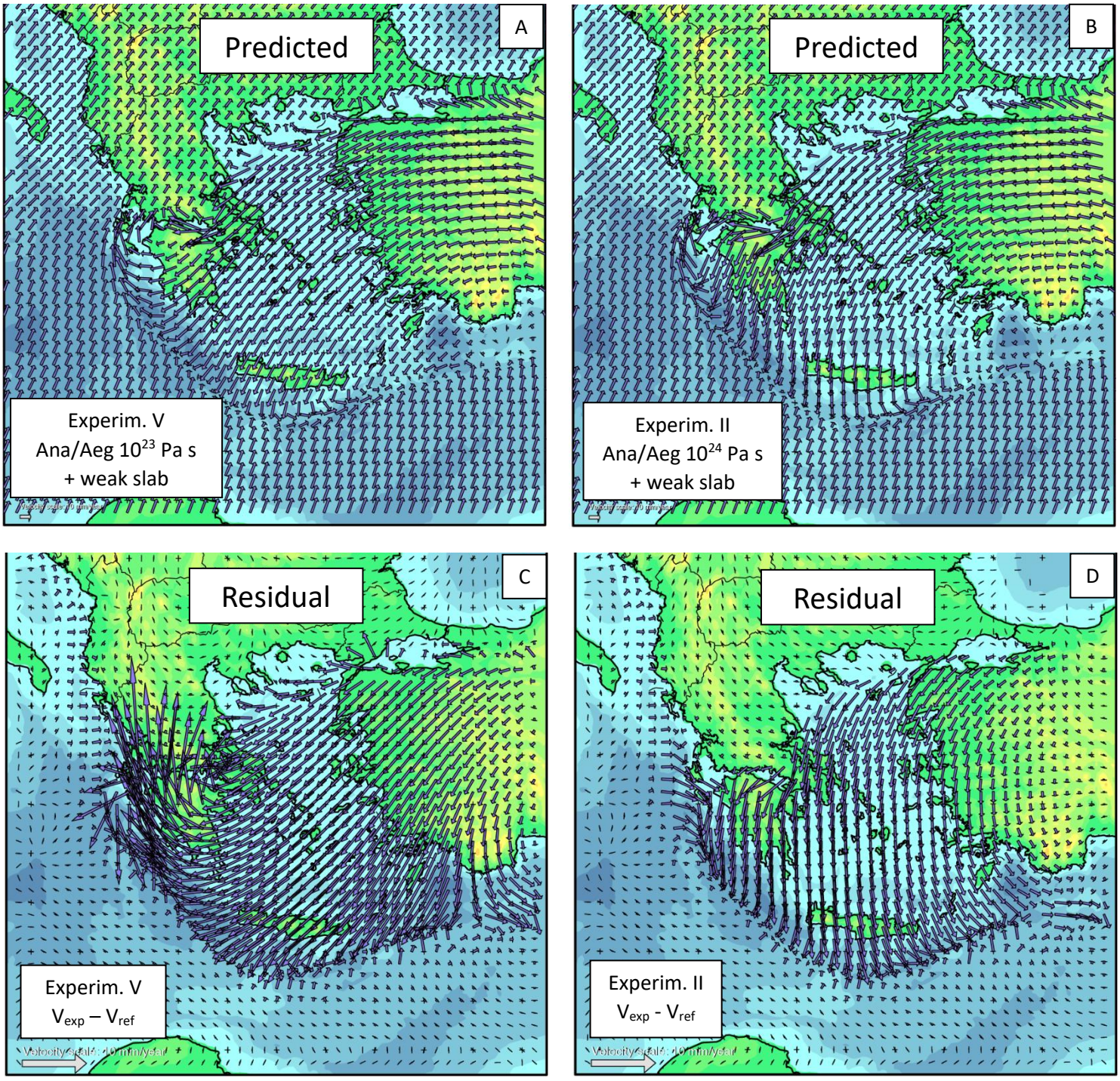

Figure 4.15 a) Experiment V predicted surface flow field, for a weakened slab and overriding plate (GMHRF)(See Table 4.3) b) Experiment II predicted surface flow field, for a weakened slab and strong overriding plate (GMHRF) c) Difference (residual) field between the reference model and experiment V. d) Difference (residual) field between the reference model and experiment II.

The result of these sensitivity tests is that a new better fitting model has been found. Figure 4.16 shows the difference between the set of experiments and the observed flow field, sorted following Table 4.3.

A strong Aegean - Anatolia plate fits the data better in the Peloponnese region (4.16b/d); The rigid lithosphere results in a more coherent movement of the Aegean and Peloponnese towards the southwest. A weak Aegean - Anatolia plate results in Peloponnese having too much westward motion (4.16a/c), which could imply Peloponnese being rheologically stronger than the central Aegean basin. A weak slab applies, in general, a south component to the velocity field of ~ 5mm yr^{-1} (4.16c-d). This improves the fit over the strong slab models run (4.16a-b). The misfit in experiment V is roughly symmetrical along a trench-perpendicular, NE oriented line centered between Peloponnese and Crete. Misfit is lowest in the center and increases towards the sides. The misfit in experiment II is lowest in the NW of the Aegean sea, increasing to the sides with its maximum in the SE. Both models II and V are improvements of the reference model and a preference for a final improved model lies in experiment V due to its symmetry.

This preferred model is left with misfit that is acceptable and misfit that invites further research. Acceptable misfit is the remainder within the Aegean region that appears to be reconcilable within the parameter space explored previously. Misfit at and around plate boundaries and weak zones are acceptable due to the limited time available for this project. Misfit that is further investigated is the sizable misfit in the mainland of Greece and North Macedonia, and the region south of Rhodos & Kephalonia.

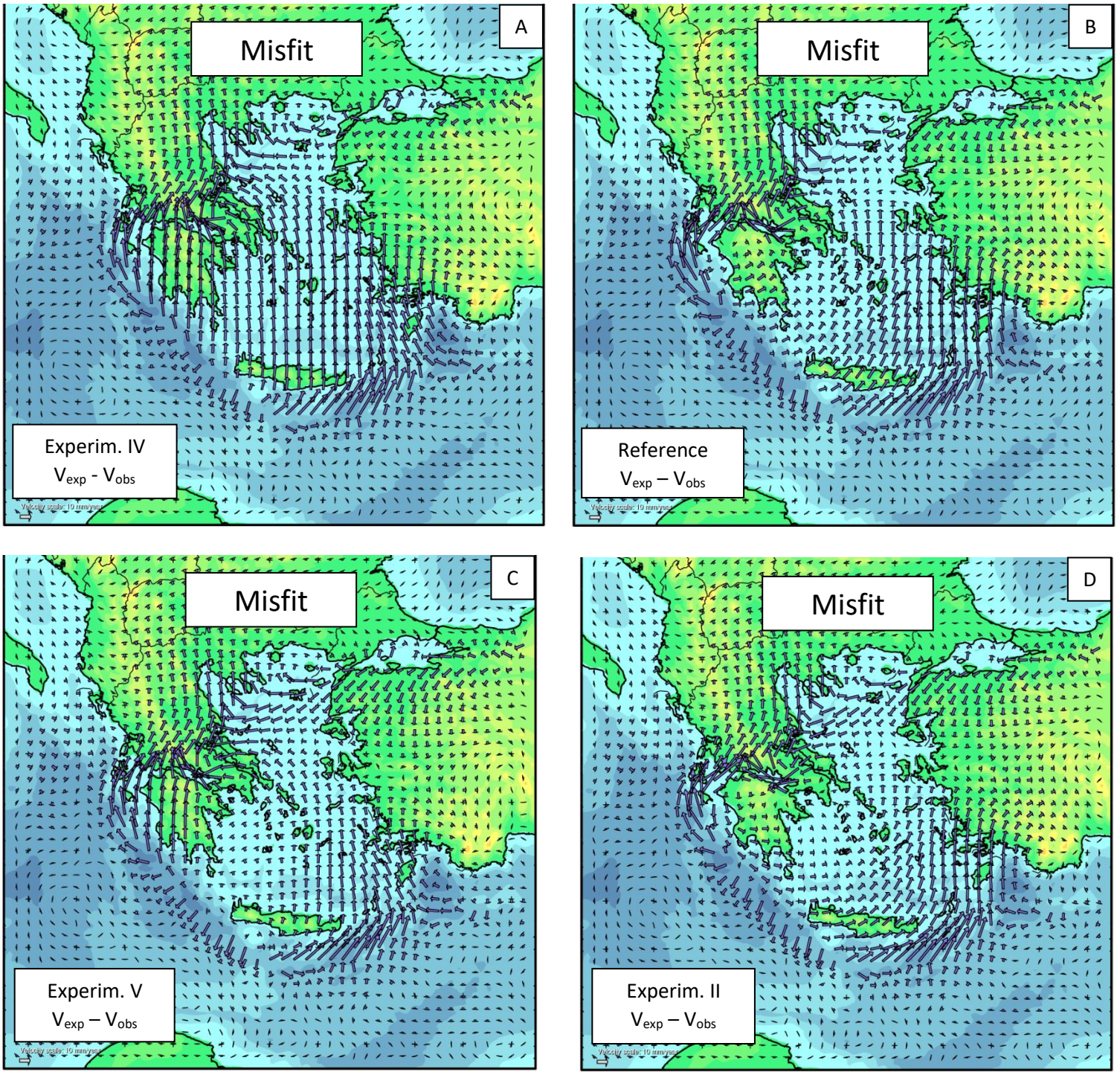

Figure 4.16 Difference between the observed GNSS surface flow field and the flow field predicted in a) experiment IV b) the reference model c) experiment V d) experiment II (Sorted following Table 4.3).

Model explorations

Following up on the findings in the previous chapter, an attempt is made to explain the misfit on the Greek mainland and North Macedonia. The Eurasian domain was separated in several subdomains: the Pannonian Basin & Carpathians, the East European platform (EEP), the Balkans and the Dinarides (60 km, 120 km, 80 km and 60 km thick, respectively) (Figure 4.17). The plastic cohesion of the Pannonian and Dinaride regions was lowered from $1*10^8$ Pa to $4*10^7$ Pa and the plastic cohesion of the Balkan region was lowered from $1*10^8$ Pa to $5*10^7$ Pa to increase susceptibility to stresses.

The results of this heterogeneous Eurasia experiment are shown in Figure 4.18a, which is comparable to the difference between the results and the reference model (Figure 4.18c) as the velocity in mainland Greece is zero in the reference model. The prediction shows the mainland of Greece moving relative to the rest of Eurasia. The direction is SW – W and ~ 15 mm yr^{-1} of magnitude, displaying an increased susceptibility to the local dynamic forcings. Comparing this to the observed field and the difference field between observed and the experiment (4.18b,d) shows that the south-component is still too low in the new model, and that the misfit in the west-direction is exasperated.

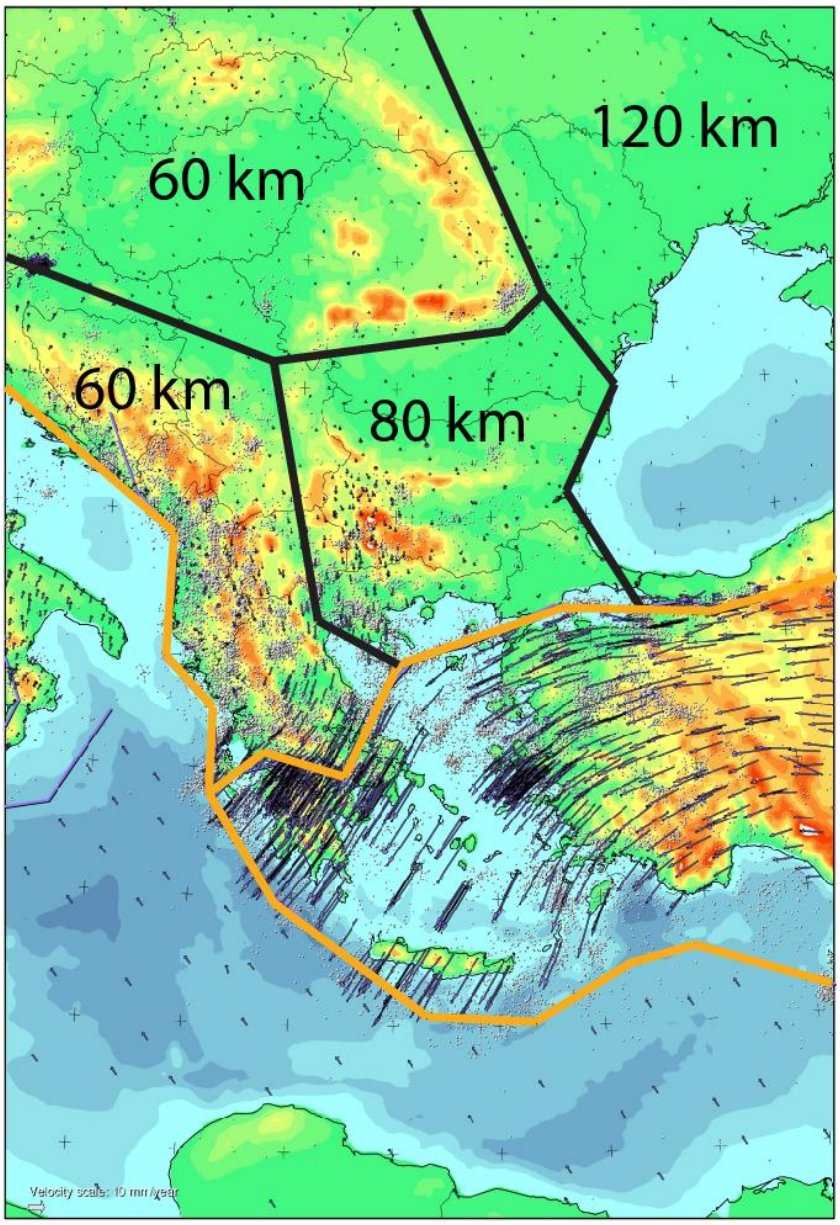

Figure 4.17 The observed GNSS surface flow field. Indicated are the subdivisions of the Eurasian continent. These are the Pannonian Basin (60 km thick), the East European Craton (120 km), the Dinarides (60 km) and the Balkans (80 km).

This mismatch can be interpreted either in context of 1) the coupling between the lithospheric domains, or 2) the effect of the mantle on the lithosphere. The observed GNSS field (Figure 4.18b) clues to the possibility that a higher NAF viscosity could better couple Greece to the Aegean - Anatolia plate; opposite sides of the NAF-Corinth weak zone show an increasing SW orientation of the velocity field from Thessaloniki to Athens. This coupling could provide a dynamic source of southward traction, dragging this domain SW. Attempts to model this have as of yet been unsuccessful. Problems arose in finding a suitable viscosity of the subdomains (which this chapter shows have yet to be optimized), a problem which is only exacerbated with the addition of further parameterization of the viscosity of (one or multiple segments of) the NAF-Corinth weak zone.

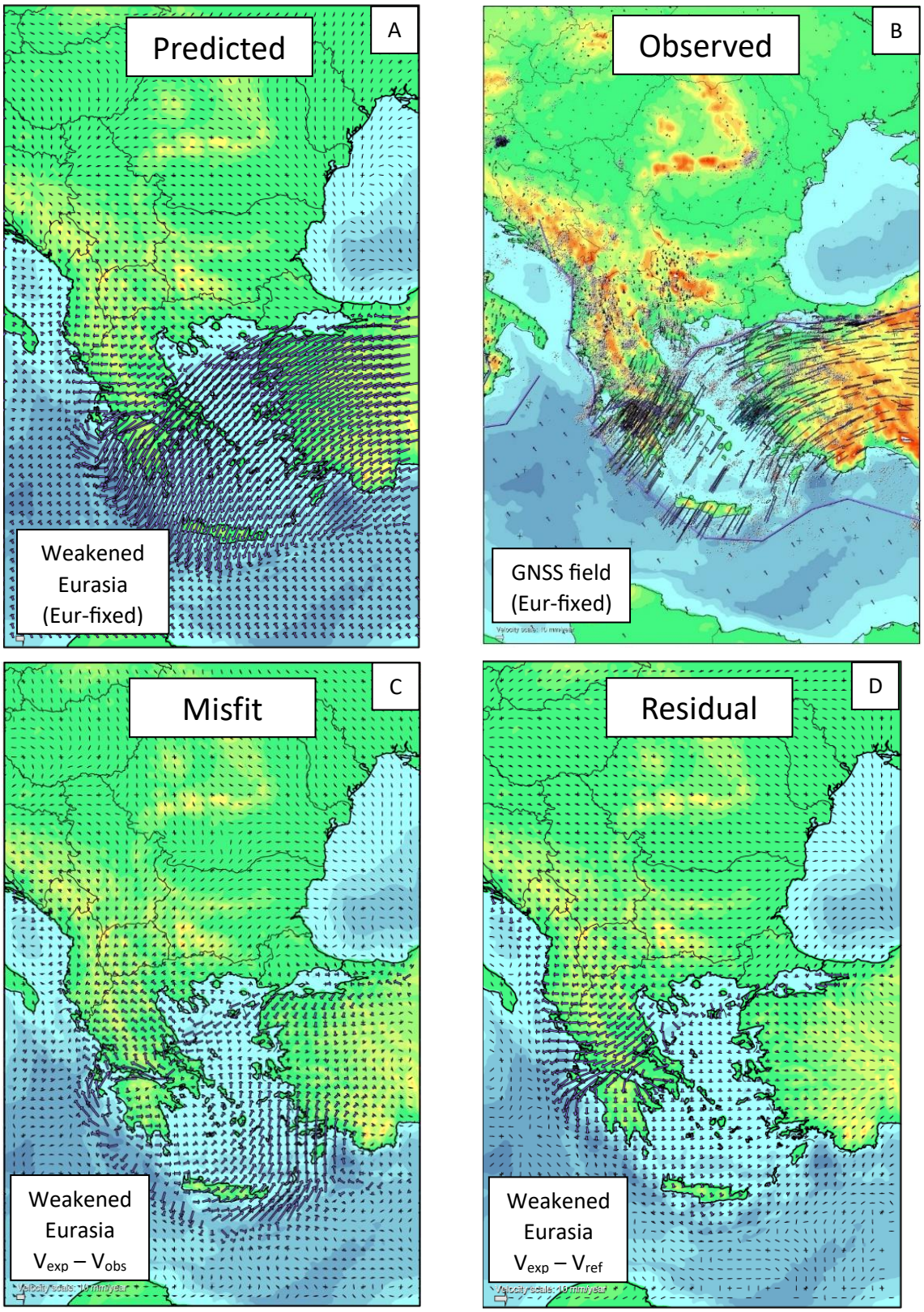

Figure 4.18 a) Predicted surface flow field, for a weakened Eurasian plate (Eurasia-fixed reference frame) b) Observed GNSS surface flow field (Eurasia-fixed reference frame) c) Difference field between the experiment and the observed field. d) Difference (residual) field between the reference model and the experiment.

Facilitating slab roll-back by implementing vertical slab tears at Rhodes deep and Kephalonia

This section addresses the misfit east of Crete and near the Gulf of Corinth stated in the last paragraph of the sensitivity test. The location of the misfit corresponds to the location of two Subduction-Transform-Edge-Propagation (STEP) Faults, at Kephalonia and Rhodos (Govers & Wortel, 2005). These faults would act as vertical separators cutting the slab and lithosphere, providing more mobility in the vertical direction for the slab to roll back and enhance S-directed flow in the Aegean region. These features are implemented in two experiments (figure 4.19a,b) as two weak zones, 120 / 200 km deep and 30 / 40 km wide, with an identical composition as the NAF, Gulf of Corinth and plate boundary weak zones.

Figure 4.19 show the results of these experiments. The difference in flow field between the reference model and the experiment are displayed. It is clear that the experiment does not (4.19a) or barely (4.19b) yield the roll-back hypothesized. Large displacement is present in the weak zones, tapering off at the sides.

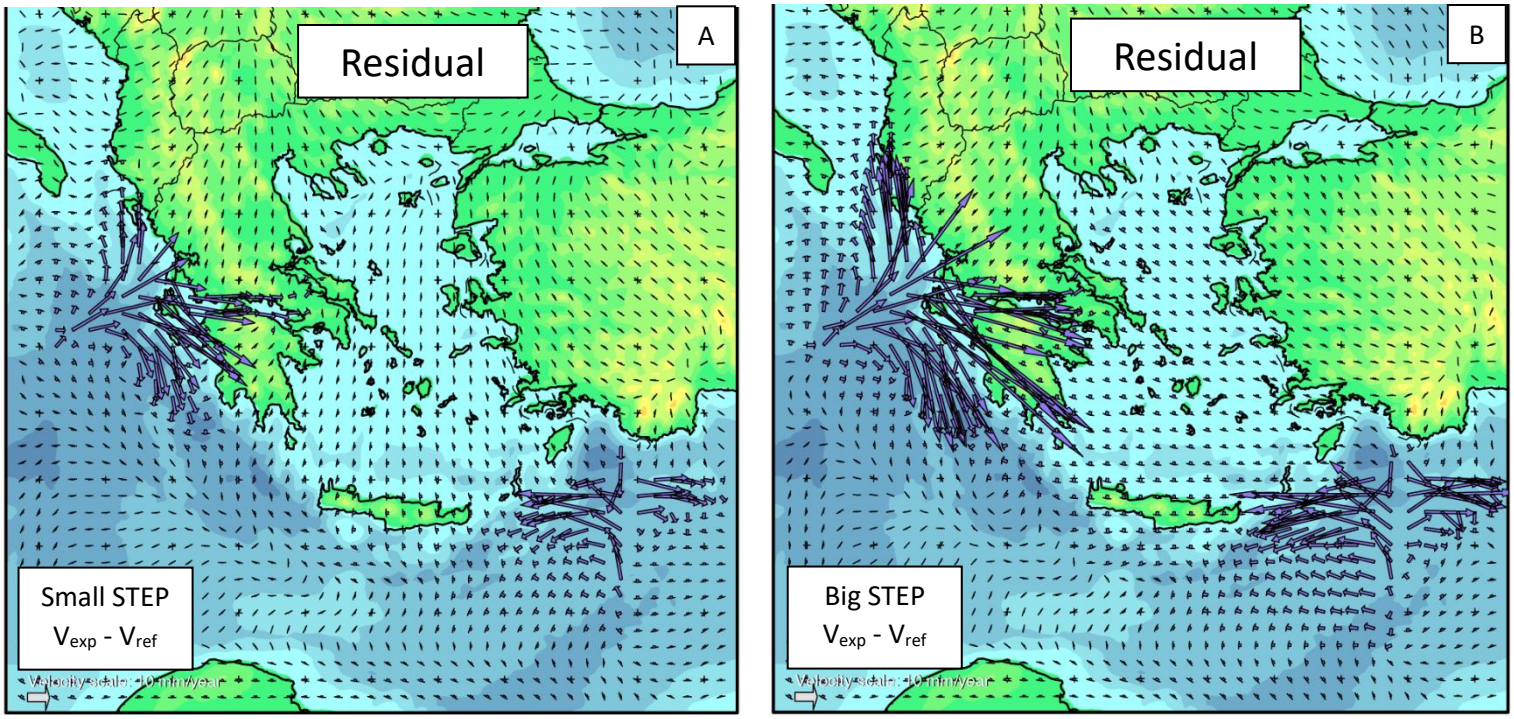

Figure 4.19 a) Difference (residual) field between the reference model and an experiment with a 120 km deep, 30 km wide STEP b) 200 km deep 40 km wide STEP

Discussion

Comment on the quality of the reference model

Misfit at Aegean slab edges

The reference model produced in this research predicts the first-order characteristics of the region. The most important deviations within the central Aegean region were reconciled with a lowered slab viscosity and lowered Aegean - Anatolia plate viscosity (Experiment V, Figure 4.16c/Figure 5.1). The remaining misfit is primarily found at the plate's sides at Peloponnese and Rhodes and directed southward. This local lack of southward flow could be caused by a lack of local rollback, but implementing STEP-faults but this did not yield the desired outcome (Figure 4.19). Further analysis in what causes this misfit could be done in the direction of regional effects. Our Aegean-Anatolia lithosphere is described as a single composition plate of 60 km with no internal weaknesses such as pre-existing fault structures, which would localise deformation (Naliboff et al., 2017). Local heterogeneities in plastic strength such as the Menderes normal fault system in west Anatolia or a better description of the Kephalonia/Gulf of Corinth faults could increase the sensitivity at Rhodos and Kephalonia to the south-directed roll-back caused by slab pull.

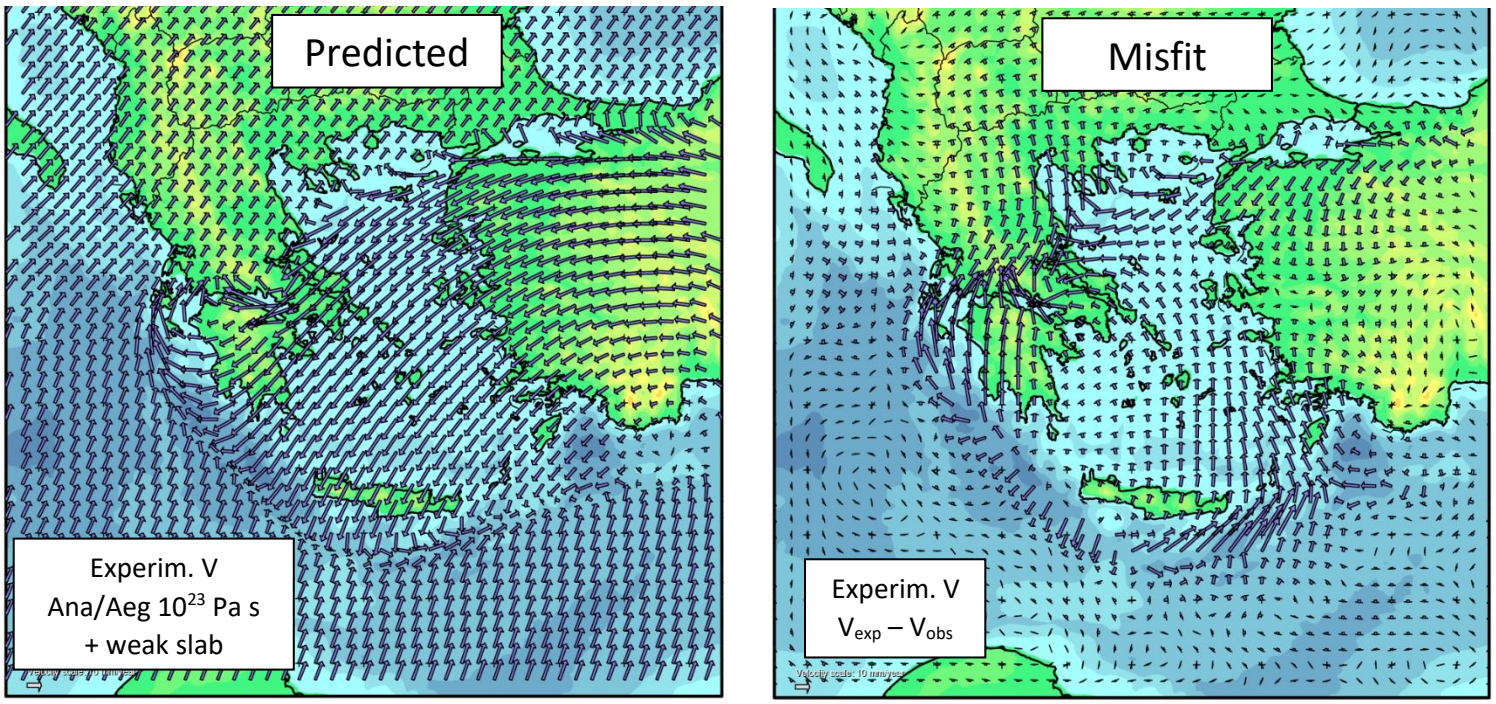

Figure 5.1 (Figure 4.16c repeated)

Misfit at mainland Greece

The similarities between the predicted mantle flow at 200 km depth (Figure 4.5) and the observed surface flow (Figure 4.1) warrant further consideration. Mantle flow at this depth displays the first-order features mentioned previously, plus a clockwise toroidal flow below the Dinarides around the Aegean slab's edge, towards the center of the Aegean slab which is not replicated in the predicted surface flow field (Figure 4.1c, at Albania/Greece). While the reference model contradicts that this flow is translated to the

surface (the predicted surface flow is markedly different from the flow at 200 km depth), a degree of uncertainty is warranted due to its limited level of refinement. In a plate-tectonic setting such as the Aegean, the prevailing convective mantle flows (which are larger than the passive flow from lithosphere friction, Figure 4.3) could hypothetically add to the surface flow by viscous coupling. One previous research found that basal flow in the Aegean region dictates its crustal movement (Carafa et al. 2015) (while this should be considered in context of other studies explaining this movement with solely lateral differences in density structure (England et al. 2016)). But this basal drag mechanism does not appear to be prominent in this reference model.

It is possible that the modelled lithosphere is too viscous as tested in the Model Explorations chapter, or that the sub-lithospheric mantle is not viscous enough. This latter explanation would reduce the coupling between lithosphere and the mantle flow and per consequence the way basal tractions from active convection are translated to the surface. Suggested follow-up experiments are to decrease the viscosity contrast between the asthenosphere and lithosphere to establish the surface flow response. The values used for these parameters in this study fall within a range of uncertainty and can therefore be used as a 'weak' benchmark from which weaker tunings can be initially disregarded in future experiments. We suggest advancing the model by increasing the activation prefactor, energy or volume of dislocation creep the upper mantle, or decreasing the power law creep exponent.

Comment on the predictions of mantle flow by the reference model

The reference model produces predictions of the mantle flow field that can be compared to seismic anisotropy maps.

We observe a trench-perpendicular flow for the mantle in the Aegean back-arc region which are associated in various other research with NE SKS splitting azimuths (Summarized in Faccenna et al. 2014, Chapter 4.2)(Figure 5.2, 5.3). The subduction and roll-back of the Aegean slab excites trench-perpendicular flow below the Aegean sea, leading to NE-SW-oriented Lattice Preferred Orientations (LPO) in olivine which are recognized in seismic anisotropy.

Our model however deviates from the hypothesis posed by previous research regarding the mantle flow pattern directly below the slab. These studies assume sub-slab mantle flow to be trench-parallel to evacuate from the backside toward the front of the backstepping slab, especially in the mantle below the Hellenides (e.g. Brun and Sokoutis, 2010). Our reference model predicts however high trench-perpendicular flows directly below the slab, as the coupling between the slab and mantle here is high. Trench-parallel flow is only observed below the Hellenic section of the slab (and at much lower velocity). The flow here may therefore not be associated to roll-back induced flow in general since the trend is not observed in the section east of Crete. A possible explanation is that the ambient mantle below the Hellenic trench is not related to this inherent back-to-front return flow, but to the absolute NNE oriented plate motion of the subducting slab,

dragging the ambient mantle in the same direction and imprinting this motion in the mantle mineral texture.

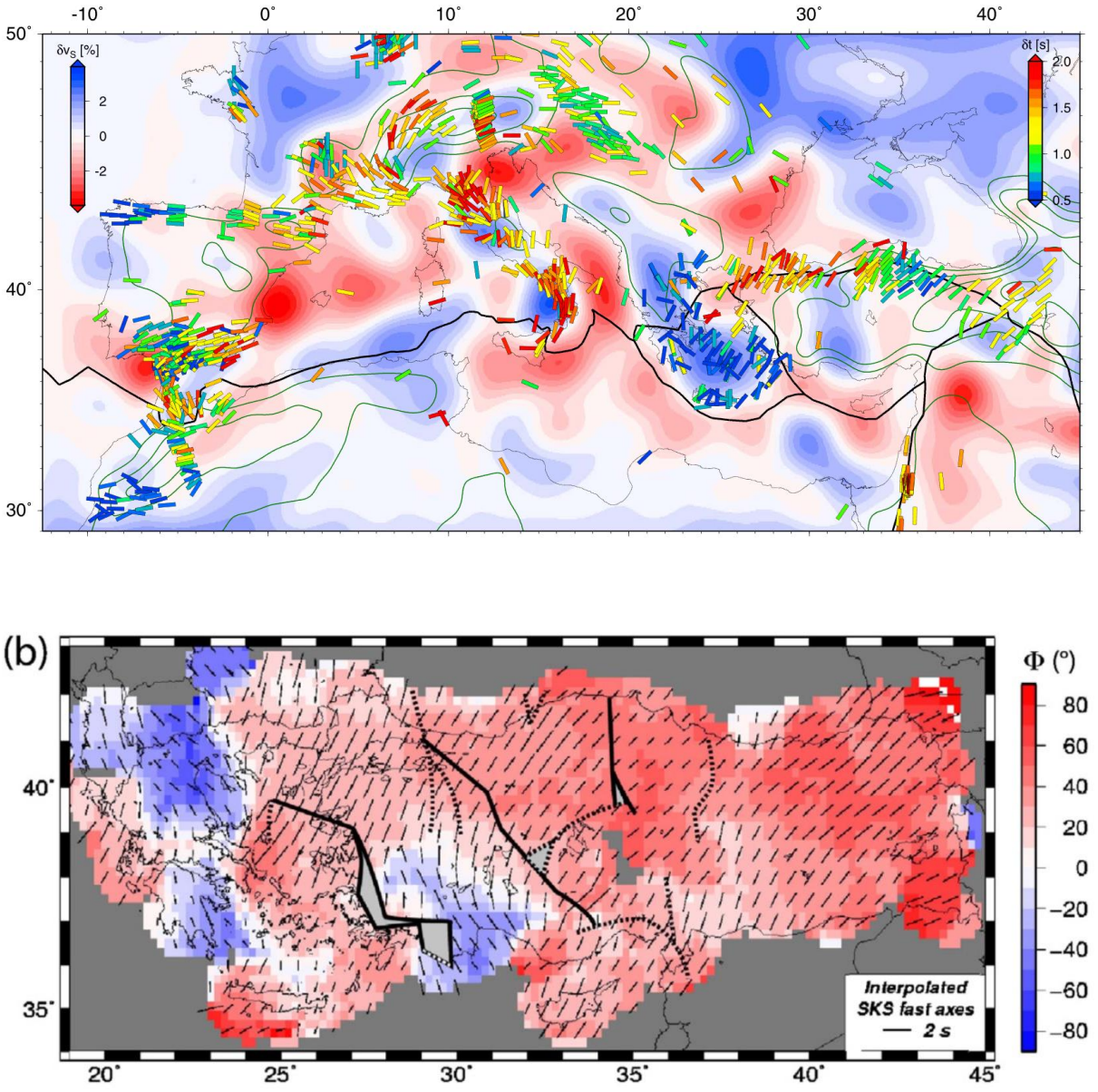

Figure 5.2 Top: seismic anisotropy distribution from shear-wave splitting (colored in delay time and oriented along fast-axis) superposed on a smoothed map of a combination of the regional tomographic image of Piromallo & Morelli (2003) and the global model of Simmons et al. (2007) averaged between 100 – 400 km (Taken from Faccenna et al. 2014). Bottom: seismic anisotropy distribution from shear-wave splitting with a background coloring indicating the interpolated azimuth (Paul et al. 2014).

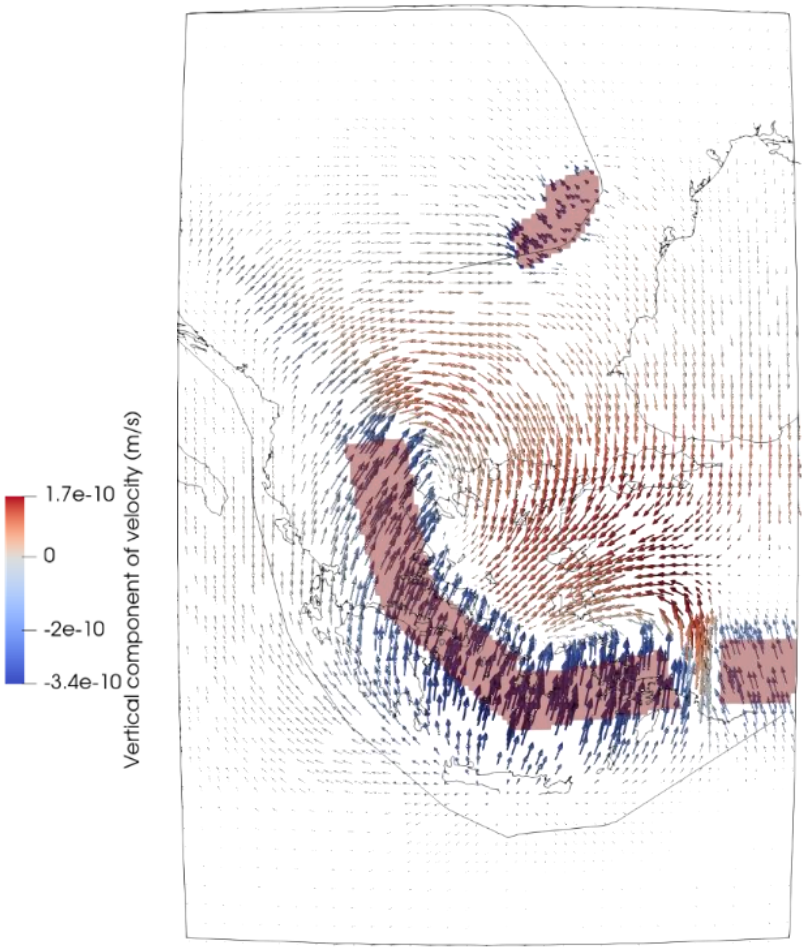

Figure 5.3 3D Mantle flow pattern prediction of the reference model at 200 km depth.

Comment on the sensitivity tests of the reference model

Slab dragging Vrancea

Both the reference model and the sensitivity test with a continuous Vrancea slab show no surface flow effect in the Vrancea zone (Figure 4.1, 4.10). However, the degree of coupling between the Vrancea slab and Eurasia makes the difference between a mantle-dragging regime or a free-sinking regime. As noted by Petrescu et al. (2021), the local seismic anisotropy direction and maximum horizontal stress direction correlate and indicate a possible relation between the ambient mantle flow and stress build-up and release. They also observe vertical tension within the slab and a transfer of the deeper compressive stresses upward to the crust, which are in favor of a continuous slab model. Our model predicts a dynamic link between the absolute plate motion of the Eurasian slab and the increased compressive horizontal stresses from the slab dragging through the upper mantle when the slab is continuous. Our model does not provide other predictions that can be linked to surface observables (i.e. uplift/subsidence rates or a detailed local stress field) but these are clear avenues for future research.

Gravitational potential energy

Our model implementation does not allow for incorporating effects of topography, therefore excluding the contribution of topography to the Gravitational Potential Energy (GPE). As the tectonic plates are modelled as homogeneous blocks of lithosphere of identical composition but varying thickness, the only GPE gradients exist at depth along the plate interfaces.

GPE effects are proposed in the literature. One 2D viscous sheet model found that GPE gradients are key in the driving of Anatolia and basal & side tractions drive the motion of the Aegean region (Carafa et al. 2015). A different study using a 2D viscous sheet model was able to fit the surface velocity field with GPE gradients in the area, without the inclusion of mantle tractions, roll-back or slab pull, but with tension along the Aegean trench south of Crete and compression along its east boundary through Anatolia (England et al. 2016). This finding is in contrast however with a geodetic strain rate analysis that does require Aegean slab roll-back (Jiménez-Munt et al. 2006). Another 2D thin sheet model does explicitly incorporate for roll-back by imposing the relative velocity between the Aegean and Nubia as a boundary condition, along with all other forces driving this roll-back (Özbakir et al., 2017). Glerum et al. (2019) suggest that the observed GPS RMS misfit is such thin sheet modelling is primarily reduced by plate boundary forces and the thin-sheet viscosity, and only secondarily by GPE forcing.

Recommendations how to advance the modelling towards a better data fit

Further investigation of implementing STEP faults or lowering Eurasia viscosity does not lead to improved roll-back or better flow field fit, respectively. It appears that the effect of the subduction of the Aegean slab affects the flow field of only the Aegean – Anatolia plate, but not the adjacent Eurasian plate. This is not expected, as the coupling between the different plates would propagate changes in flow field. An analysis on the mechanical equilibrium of the Eurasian plate led to the conclusion that, although mantle flow and lithospheric body forces are dominant drivers, the collision of Africa on Eurasia's south border is a significant contribution in the absolute northward direction of the Eurasian plate (Warners-Ruckstuhl et al. 2012).

This model possibly suffers in the degree of coupling between the individual plates due to a high viscosity contrast at the plate boundary weak zones. The viscosity of our lithosphere is realistic (maximized at $5*10^{23}$ Pa s, oceanic lithosphere is possibly 10^{23} to 10^{24} Pa s (Burov, 2011), a factor of 10^4 higher than asthenosphere (10^{19}-$5*10^{19}$ Pa s)), and much higher than the effective viscosity of ~ 10^{21} - 10^{22} Pa s found by England et al. (2016). The question whether the plates are too viscous is also tendentious in the light that previous authors concluded that the geodetic velocity field is best represented by undeformable blocks separated by weak zones <<100 km wide (Reilinger et al., 2006). We recommend implementing additional weak zones between north and central Greece, and between Anatolia & Aegean sensu the "hybrid dynamic" sheet model used by Carafa et al. (2015)(Figure 5.4 left), with which they adequately reproduce the flow field at mainland Greece and acceleration towards the Hellenic trench (Figure 5.4 right).

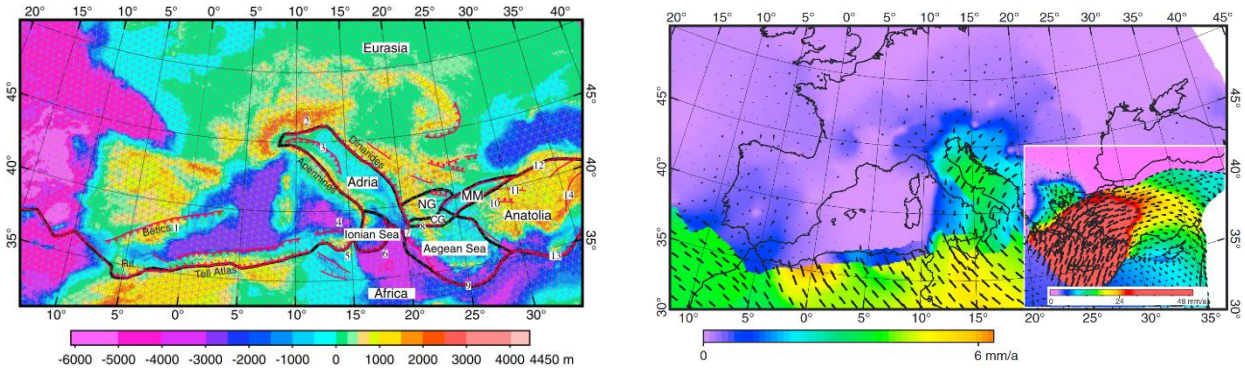

Figure 5.4 Left: Model topography by Carafa et al. (2015), with weak zones indicated in red. Right: Preferred model output by Carafa et al. (2015).

Conclusion

This research uses a 3D instantaneous dynamics model of subduction in the Aegean and Vrancea regions to reproduce and analyze surface flow. The reference model reproduces the first-order features of the region's observed surface flow field. Anatolia displays westward movement, rotating counterclockwise to a SW, trench-parallel orientation in the Aegean region and Peloponnese. The Eurasian and African plates move as coherent blocks NE in the Global Mantle Hotspot Reference Frame (GMHRF), a movement in which the Vrancea slab does not show an effect on the local crustal flow pattern. The predictions of the reference model show that flow in the mantle is dominated by the roll-back of the Aegean slab. At 200 km depth, flow converges to the center of the slab, filling in the space created by its sinking. Flow velocities decrease dramatically deeper into the upper mantle, and its flow pattern is generally diverging away from the slab or oriented upward in a poloidal flow manner.

The sensitivity tests conducted on the reference model are, in order of importance on the surface flow field: 1) the presence of the Aegean slab, 2) the viscosity of the subducting Aegean slab, 3) the viscosity of the Aegean - Anatolia plate, 4) the viscosity of the plate boundary interface, and 5) the coupling of the Vrancea slab. The degree of coupling of the Vrancea slab to the Eurasian plate is not recognized in the predicted surface flow field. The mantle impact of a continuous/detached regime is significant, as a detached Vrancea slab displays vertical sinking, whereas the continuous Vrancea slab is predicted to be dragged through the mantle. This bears consequences on the friction from slab dragging resistance and an accompanying increase in horizontal compression on the slab, possibly increasing the seismicity in the Vrancea slab (Petrescu et al. 2021).

Misfit in the reference model appears to be refinable using the parameter space explored in the Sensitivity Tests subsection, except for two features: misfit on the Eurasian plate on the mainland of Greece, and the general misfit in magnitude of roll-back of the Aegean region, specifically at the Aegean slab edges. Two subsequent tests were conducted 1) to increase the susceptibility of Eurasia to changes in its surface flow field by subdividing the plate into 4 regions of varying depth and viscosity and 2) to try and explain the remaining misfit within the Aegean region by implementing vertical lithosphere-piercing weak zones imitating STEP-faults at Kephalonia and the Rhodos Deep. The lowering of Eurasia's viscosity has the potential to better fit the surface flow field of mainland Greece but needs to be further analyzed in a parameter space that includes the viscosity contrast between & coupling of the main tectonic plates. The implementation of the vertical weak zones does not provide the magnitude of roll-back required, nor indicate insightful changes to the surface flow pattern. Further model advancements should be sought in the coupling between the different tectonic plates and in more heterogeneity of the lithosphere both in plastic strength as well as lateral density structure. This 3D model provides valuable new insight in the interactions between mantle flow and seismic anisotropy patterns, as well as the interactions between convective mantle flow, basal tractions on the lithosphere and the surface flow field.

Acknowledgements

This work of research finalizes my Master's degree and I would like to express my gratitude to several individuals who helped me and contributed greatly in making this work possible. I would like thank Prof. Dr. Wim Spakman for both his unwavering support & guidance throughout our time working together and his unparalleled geodynamic insight from which I have learned so much. I thank Prof. Dr. Cedric Thieulot for his support on the technical side of geodynamic modelling as well as his ever-relaxed attitude. My gratitude goes out to Erik van der Wiel MSc who both at the start of my studies as now at the end taught me how to interpret physics both in how complex it is and yet how it can be explained in very simple terms. Thanks for giving me the opportunity to present my research at NAC. I want to thank Dr. Anne Glerum for paving the way in 3D instantaneous dynamics modelling of the Aegean with her stellar thesis, and Dr. Menno Fraters for creating the Geodynamic World Builder with which my favorite geophysical subject – subduction modelling – has become as tangible and intuitive as playing a video game. Last but definitely not least I want to express my deepest thanks to my colleague and friend Lex Verbrugh MSc. After our many collaborations in the Master, Lex pioneered geodynamic modelling using the GWB for his own thesis and took me under his wing when I started my project on the other side of the Mediterranean. His proactive attitude, genuine curiosity and drive to make not only himself but everyone he works with succeed, are laudable character traits that promise great things for the future and I thank him for all his support.

References

Amaru, M., 2007. Global travel time tomography with 3-D reference models = Globale reistijdentomografie met 3-D referentiemodellen. Faculteit Geowetenschappen Univ. Utrecht, Utrecht.

Baron, J., Morelli, A., 2017. Full-waveform seismic tomography of the Vrancea, Romania, subduction region. Physics of the Earth and Planetary Interiors 273, 36–49. https://doi.org/10.1016/j.pepi.2017.10.009

Berk Biryol, C., Beck, S.L., Zandt, G., Özacar, A.A., 2011. Segmented African lithosphere beneath the Anatolian region inferred from teleseismic P-wave tomography: Segmented lithosphere beneath Anatolia. Geophysical Journal International 184, 1037–1057. https://doi.org/10.1111/j.1365-246X.2010.04910.x

Bijwaard, H., Spakman, W., Engdahl, E.R., 1998. Closing the gap between regional and global travel time tomography. Journal of Geophysical Research: Solid Earth 103, 30055–30078. https://doi.org/10.1029/98JB02467

Bird, P., 1998. Kinematic history of the Laramide orogeny in latitudes 35°–49°N, western United States. Tectonics 17, 780–801. https://doi.org/10.1029/98TC02698

Bokelmann, G., Rodler, F.-A., 2014. Nature of the Vrancea seismic zone (Eastern Carpathians) – New constraints from dispersion of first-arriving P-waves. Earth and Planetary Science Letters 390, 59–68. https://doi.org/10.1016/j.epsl.2013.12.034

Brun, J.-P., Faccenna, C., Gueydan, F., Sokoutis, D., Philippon, M., Kydonakis, K., Gorini, C., 2016. The two-stage Aegean extension, from localized to distributed, a result of slab rollback acceleration. Canadian Journal of Earth Sciences 53. https://doi.org/10.1139/cjes-2015-0203

Brun, J.-P., Sokoutis, D., 2010. 45 m.y. of Aegean crust and mantle flow driven by trench retreat. Geology 38, 815–818. https://doi.org/10.1130/G30950.1

Burov, E.B., 2011. Rheology and strength of the lithosphere. Marine and Petroleum Geology 28, 1402–1443. https://doi.org/10.1016/j.marpetgeo.2011.05.008

Carafa, M.M.C., Barba, S., Bird, P., 2015. Neotectonics and long-term seismicity in Europe and the Mediterranean region. Journal of Geophysical Research: Solid Earth 120, 5311–5342. https://doi.org/10.1002/2014JB011751

Chertova, M.V., Geenen, T., van den Berg, A., Spakman, W., 2012. Using open sidewalls for modelling self-consistent lithosphere subduction dynamics. Solid Earth 3, 313–326. https://doi.org/10.5194/se-3-313-2012

Cloetingh, S.A.P.L., Burov, E., Matenco, L., Toussaint, G., Bertotti, G., Andriessen, P.A.M., Wortel, M.J.R., Spakman, W., 2004. Thermo-mechanical controls on the mode of continental collision in the SE Carpathians (Romania). Earth and Planetary Science Letters 218, 57–76. https://doi.org/10.1016/S0012-821X(03)00645-9

De Boorder, H., Spakman, W., White, S.H., Wortel, M.J.R., 1998. Late Cenozoic mineralization, orogenic collapse and slab detachment in the European Alpine Belt. Earth and Planetary Science Letters 164, 569–575. https://doi.org/10.1016/S0012-821X(98)00247-7

Doubrovine, P.V., Steinberger, B., Torsvik, T.H., 2012. Absolute plate motions in a reference frame defined by moving hot spots in the Pacific, Atlantic, and Indian oceans. Journal of Geophysical Research: Solid Earth 117. https://doi.org/10.1029/2011JB009072

El-Sharkawy, A., Meier, T., Lebedev, S., Behrmann, J.H., Hamada, M., Cristiano, L., Weidle, C., Köhn, D., 2020. The Slab Puzzle of the Alpine-Mediterranean Region: Insights From a New, High-Resolution, Shear Wave Velocity Model of the Upper Mantle. Geochemistry, Geophysics, Geosystems 21, e2020GC008993. https://doi.org/10.1029/2020GC008993

Endrun, B., Lebedev, S., Meier, T., Tirel, C., Friederich, W., 2011. Complex layered deformation within the Aegean crust and mantle revealed by seismic anisotropy. Nature Geosci 4, 203–207. https://doi.org/10.1038/ngeo1065

England, P., Houseman, G., Nocquet, J.-M., 2016. Constraints from GPS measurements on the dynamics of deformation in Anatolia and the Aegean. Journal of Geophysical Research: Solid Earth 121, 8888–8916. https://doi.org/10.1002/2016JB013382

Faccenna, C., Becker, T.W., Auer, L., Billi, A., Boschi, L., Brun, J.P., Capitanio, F.A., Funiciello, F., Horvàth, F., Jolivet, L., Piromallo, C., Royden, L., Rossetti, F., Serpelloni, E., 2014. Mantle dynamics in the Mediterranean: MEDITERRANEAN DYNAMIC. Rev. Geophys. 52, 283–332. https://doi.org/10.1002/2013RG000444

Fraters, M., Thieulot, C., Van Den Berg, A., Spakman, W., 2019. The Geodynamic World Builder: a solution for complex initial conditions in numerical modeling. Solid Earth 10, 1785–1807.

Fuchs, K., Bonjer, K.-P., Bock, G., Cornea, I., Radu, C., Enescu, D., Jianu, D., Nourescu, A., Merkler, G., Moldoveanu, T., Tudorache, G., 1979. The Romanian earthquake of March 4, 1977 ii. Aftershocks and migration of seismic activity +. Tectonophysics, Proceedings of the 16th General Assemble of the European Seismological Commission 53, 225–247. https://doi.org/10.1016/0040-1951(79)90068-4

Garel, F., Goes, S., Davies, D.R., Davies, J.H., Kramer, S.C., Wilson, C.R., 2014. Interaction of subducted slabs with the mantle transition-zone: A regime diagram from 2-D thermo-mechanical models with a mobile trench and an overriding plate. Geochemistry, Geophysics, Geosystems 15, 1739–1765. https://doi.org/10.1002/2014GC005257

Gîrbacea, R., Frisch, W., 1998. Slab in the wrong place: Lower lithospheric mantle delamination in the last stage of the Eastern Carpathian subduction retreat. Geol 26, 611. https://doi.org/10.1130/0091-7613(1998)026<0611:SITWPL>2.3.CO;2

Glerum, A.C., Spakman, W., Universiteit Utrecht, Faculteit Geowetenschappen, 2019. Geodynamics of complex plate boundary regions: insights from numerical models of convergent eastern Mediterranean and divergent east African plate tectonics = Geodynamica van complexe plaatgrenzen : inzichten verkregen uit numerieke modellen van de plaattektoniek van het oostelijk Middellandse Zeegebied en de Oost-Afrikaanse Rift. Utrecht University, Faculty of Geosciences, Department of Earth Sciences, Utrecht.

Göğüş, O.H., Pysklywec, R.N., Faccenna, C., 2016. Postcollisional lithospheric evolution of the Southeast Carpathians: Comparison of geodynamical models and observations. Tectonics 35, 1205–1224. https://doi.org/10.1002/2015TC004096

Govers, R., Wortel, M.J.R., 2005. Lithosphere tearing at STEP faults: response to edges of subduction zones. Earth and Planetary Science Letters 236, 505–523. https://doi.org/10.1016/j.epsl.2005.03.022

Hall, R., Spakman, W., 2015. Mantle structure and tectonic history of SE Asia. Tectonophysics 658, 14–45. https://doi.org/10.1016/j.tecto.2015.07.003

Handy, M.R., Giese, J., Schmid, S.M., Pleuger, J., Spakman, W., Onuzi, K., Ustaszewski, K., 2019. Coupled Crust-Mantle Response to Slab Tearing, Bending, and Rollback Along the Dinaride-Hellenide Orogen. Tectonics 38, 2803–2828. https://doi.org/10.1029/2019TC005524

Handy, M.R., M. Schmid, S., Bousquet, R., Kissling, E., Bernoulli, D., 2010. Reconciling plate-tectonic reconstructions of Alpine Tethys with the geological–geophysical record of spreading and subduction in the Alps. Earth-Science Reviews 102, 121–158. https://doi.org/10.1016/j.earscirev.2010.06.002

Hirth, G., Kohlstedt, D., 2003. Rheology of the upper mantle and the mantle wedge: A view from the experimentalists, in: Eiler, J. (Ed.), Geophysical Monograph Series. American Geophysical Union, Washington, D. C., pp. 83–105. https://doi.org/10.1029/138GM06

Jolivet, L., Faccenna, C., Huet, B., Labrousse, L., Le Pourhiet, L., Lacombe, O., Lecomte, E., Burov, E., Denèle, Y., Brun, J.-P., Philippon, M., Paul, A., Salaün, G., Karabulut, H., Piromallo, C., Monié, P., Gueydan, F., Okay, A.I., Oberhänsli, R., Pourteau, A., Augier, R., Gadenne, L., Driussi, O., 2013. Aegean tectonics: Strain localisation, slab tearing and trench retreat. Tectonophysics 597–598, 1–33. https://doi.org/10.1016/j.tecto.2012.06.011

Karabulut, H., Paul, A., Özbakır, A.D., Ergün, T., Şentürk, S., 2019. A new crustal model of the Anatolia–Aegean domain: evidence for the dominant role of isostasy in the support of the Anatolian plateau. Geophysical Journal International 218, 57–73. https://doi.org/10.1093/gji/ggz147

Katsura, T., 2022. A Revised Adiabatic Temperature Profile for the Mantle. JGR Solid Earth 127. https://doi.org/10.1029/2021JB023562

Knapp, J.H., Knapp, C.C., Raileanu, V., Matenco, L., Mocanu, V., Dinu, C., 2005. Crustal constraints on the origin of mantle seismicity in the Vrancea Zone, Romania: The case for active continental lithospheric delamination. Tectonophysics, The Carpathians-Pannonian Basin System 410, 311–323. https://doi.org/10.1016/j.tecto.2005.02.020

Koulakov, I., Zaharia, B., Enescu, B., Radulian, M., Popa, M., Parolai, S., Zschau, J., 2010. Delamination or slab detachment beneath Vrancea? New arguments from local

earthquake tomography. Geochemistry, Geophysics, Geosystems 11. https://doi.org/10.1029/2009GC002811
Kreemer, C., Blewitt, G., Klein, E.C., 2014. A geodetic plate motion and Global Strain Rate Model. Geochemistry, Geophysics, Geosystems 15, 3849–3889. https://doi.org/10.1002/2014GC005407
Kronbichler, M., Heister, T., Bangerth, W., 2012. High accuracy mantle convection simulation through modern numerical methods. Geophysical Journal International 191, 12–29. https://doi.org/10.1111/j.1365-246X.2012.05609.x
Lechmann, S.M., May, D.A., Kaus, B.J.P., Schmalholz, S.M., 2011. Comparing thin-sheet models with 3-D multilayer models for continental collision. Geophysical Journal International 187, 10–33. https://doi.org/10.1111/j.1365-246X.2011.05164.x
Marović, M., Djoković, I., Pešić, L., Radovanović, S., Toljić, M., Gerzina, N., 2002. Neotectonics and seismicity of the southern margin of the Pannonian basin in Serbia. Stephan Mueller Spec. Publ. Ser. 3, 277–295. https://doi.org/10.5194/smsps-3-277-2002
Martin, M., Wenzel, F., CALIXTO working group, 2006. High-resolution teleseismic body wave tomography beneath SE-Romania - II. Imaging of a slab detachment scenario. Geophysical Journal International 164, 579–595. https://doi.org/10.1111/j.1365-246X.2006.02884.x
Matenco, L., Radivojević, D., 2012. On the formation and evolution of the Pannonian Basin: Constraints derived from the structure of the junction area between the Carpathians and Dinarides. Tectonics 31. https://doi.org/10.1029/2012TC003206
McClusky, S., Balassanian, S., Barka, A., Demir, C., Ergintav, S., Georgiev, I., Gurkan, O., Hamburger, M., Hurst, K., Kahle, H., Kastens, K., Kekelidze, G., King, R., Kotzev, V., Lenk, O., Mahmoud, S., Mishin, A., Nadariya, M., Ouzounis, A., Paradissis, D., Peter, Y., Prilepin, M., Reilinger, R., Sanli, I., Seeger, H., Tealeb, A., Toksöz, M.N., Veis, G., 2000. Global Positioning System constraints on plate kinematics and dynamics in the eastern Mediterranean and Caucasus. Journal of Geophysical Research: Solid Earth 105, 5695–5719. https://doi.org/10.1029/1999JB900351
McKenzie, D.P., 1969. Speculations on the Consequences and Causes of Plate Motions*. Geophysical Journal International 18, 1–32. https://doi.org/10.1111/j.1365-246X.1969.tb00259.x
Métois, M., D'Agostino, N., Avallone, A., Chamot-Rooke, N., Rabaute, A., Duni, L., Kuka, N., Koci, R., Georgiev, I., 2015. Insights on continental collisional processes from GPS data: Dynamics of the peri-Adriatic belts. Journal of Geophysical Research: Solid Earth 120, 8701–8719. https://doi.org/10.1002/2015JB012023
Naliboff, J.B., Buiter, S.J.H., Péron-Pinvidic, G., Osmundsen, P.T., Tetreault, J., 2017. Complex fault interaction controls continental rifting. Nat Commun 8, 1179. https://doi.org/10.1038/s41467-017-00904-x
Nocquet, J.-M., 2012. Present-day kinematics of the Mediterranean: A comprehensive overview of GPS results. Tectonophysics, Orogenic processes and structural heritage in Alpine-type mountain belts 579, 220–242. https://doi.org/10.1016/j.tecto.2012.03.037
Oncescu, M.-C., Bonjer, K.-P., 1997. A note on the depth recurrence and strain release of large Vrancea earthquakes. Tectonophysics, Tectonics of the Alpine-Carpathian-Pannonian Region, II 272, 291–302. https://doi.org/10.1016/S0040-1951(96)00263-6

Özbakir, A.D., Govers, R., Wortel, R., 2017. Active faults in the Anatolian-Aegean plate boundary region with Nubia. Turkish J Earth Sci 26, 30–56. https://doi.org/10.3906/yer-1603-4

Özbakır, A.D., Govers, R., Fichtner, A., 2020. The Kefalonia Transform Fault: A STEP fault in the making. Tectonophysics 787, 228471. https://doi.org/10.1016/j.tecto.2020.228471

Petrescu, L., Borleanu, F., Radulian, M., Ismail-Zadeh, A., Maţenco, L., 2021. Tectonic regimes and stress patterns in the Vrancea Seismic Zone: Insights into intermediate-depth earthquake nests in locked collisional settings. Tectonophysics 799, 228688. https://doi.org/10.1016/j.tecto.2020.228688

Piña-Valdés, J., Socquet, A., Beauval, C., Doin, M.-P., D'Agostino, N., Shen, Z.-K., 2022. 3D GNSS Velocity Field Sheds Light on the Deformation Mechanisms in Europe: Effects of the Vertical Crustal Motion on the Distribution of Seismicity. Journal of Geophysical Research: Solid Earth 127, e2021JB023451. https://doi.org/10.1029/2021JB023451

Piromallo, C., Morelli, A., 2003. *P* wave tomography of the mantle under the Alpine-Mediterranean area: P WAVE TOMOGRAPHY OF THE MANTLE. J. Geophys. Res. 108. https://doi.org/10.1029/2002JB001757

Reilinger, R., McClusky, S., Vernant, P., Lawrence, S., Ergintav, S., Cakmak, R., Ozener, H., Kadirov, F., Guliev, I., Stepanyan, R., Nadariya, M., Hahubia, G., Mahmoud, S., Sakr, K., ArRajehi, A., Paradissis, D., Al-Aydrus, A., Prilepin, M., Guseva, T., Evren, E., Dmitrotsa, A., Filikov, S.V., Gomez, F., Al-Ghazzi, R., Karam, G., 2006. GPS constraints on continental deformation in the Africa-Arabia-Eurasia continental collision zone and implications for the dynamics of plate interactions: EASTERN MEDITERRANEAN ACTIVE TECTONICS. J. Geophys. Res. 111, n/a-n/a. https://doi.org/10.1029/2005JB004051

Schmid, S.M., Fügenschuh, B., Kounov, A., Maţenco, L., Nievergelt, P., Oberhänsli, R., Pleuger, J., Schefer, S., Schuster, R., Tomljenović, B., Ustaszewski, K., van Hinsbergen, D.J.J., 2020. Tectonic units of the Alpine collision zone between Eastern Alps and western Turkey. Gondwana Research 78, 308–374. https://doi.org/10.1016/j.gr.2019.07.005

Serpelloni, E., Cavaliere, A., Martelli, L., Pintori, F., Anderlini, L., Borghi, A., Randazzo, D., Bruni, S., Devoti, R., Perfetti, P., Cacciaguerra, S., 2022. Surface Velocities and Strain-Rates in the Euro-Mediterranean Region From Massive GPS Data Processing. Front. Earth Sci. 10, 907897. https://doi.org/10.3389/feart.2022.907897

Spakman, W., van der Lee, S., van der Hilst, R., 1993. Travel-time tomography of the European-Mediterranean mantle down to 1400 km. Physics of the Earth and Planetary Interiors 79, 3–74. https://doi.org/10.1016/0031-9201(93)90142-V

Spakman, W., Wortel, M.J.R., Vlaar, N.J., 1988. The Hellenic Subduction Zone: A tomographic image and its geodynamic implications. Geophys. Res. Lett. 15, 60–63. https://doi.org/10.1029/GL015i001p00060

Sperner, B., Lorenz, F., Bonjer, K., Hettel, S., Müller, B., Wenzel, F., 2001. Slab break-off – abrupt cut or gradual detachment? New insights from the Vrancea Region (SE Carpathians, Romania). Terra Nova 13, 172–179. https://doi.org/10.1046/j.1365-3121.2001.00335.x

van der Meer, D.G., Douwe J.J. van Hinsbergen, Spakman, W., 2018. Atlas of the underworld: Slab remnants in the mantle, their sinking history, and a new outlook on lower mantle viscosity. Tectonophysics 723, 309–448. https://doi.org/10.1016/j.tecto.2017.10.004

van Hinsbergen, D.J.J., Hafkenscheid, E., Spakman, W., Meulenkamp, J.E., Wortel, R., 2005. Nappe stacking resulting from subduction of oceanic and continental lithosphere below Greece. Geol 33, 325. https://doi.org/10.1130/G20878.1

van Hinsbergen, D.J.J., Schmid, S.M., 2012. Map view restoration of Aegean–West Anatolian accretion and extension since the Eocene. Tectonics 31. https://doi.org/10.1029/2012TC003132

van Hinsbergen, D.J.J., Torsvik, T.H., Schmid, S.M., Maţenco, L.C., Maffione, M., Vissers, R.L.M., Gürer, D., Spakman, W., 2020. Orogenic architecture of the Mediterranean region and kinematic reconstruction of its tectonic evolution since the Triassic. Gondwana Research 81, 79–229. https://doi.org/10.1016/j.gr.2019.07.009

Verbrugh, A. L., Spakman, W., 2023. Master Thesis, A new modelling approach for the Gibraltar arc region: 3D instantaneous dynamics modelling.

Warners-Ruckstuhl, K.N., Govers, R., Wortel, R., 2012. Lithosphere–mantle coupling and the dynamics of the Eurasian Plate. Geophysical Journal International 189, 1253–1276. https://doi.org/10.1111/j.1365-246X.2012.05427.x

Weidle, C., Widiyantoro, S., CALIXTO Working Group, 2005. Improving depth resolution of teleseismic tomography by simultaneous inversion of teleseismic and global *P* -wave traveltime data-application to the Vrancea region in Southeastern Europe. Geophysical Journal International 162, 811–823. https://doi.org/10.1111/j.1365-246X.2005.02649.x

Wortel, M.J.R., Spakman, W., 2000. Subduction and Slab Detachment in the Mediterranean-Carpathian Region. Science 290, 1910–1917. https://doi.org/10.1126/science.290.5498.1910